Full one-loop electro-weak corrections to three-jet observables at the *Z* pole and beyond

Full one-loop electro-weak corrections to three-jet observables at the Z pole and beyond

C.M. Carloni-Calame,[a,b] **S. Moretti,**[b,c] **F. Piccinini**[d] **and D.A. Ross**[b,e]

[a]*INFN,*
 via E. Fermi 40, Frascati, Italy

[b]*School of Physics and Astronomy, University of Southampton,*
 Highfield, Southampton SO17 1BJ, U.K.

[c]*Laboratoire de Physique Theorique, Universite de Paris-Sud XI,*
 Batiment 210, F-91405 Orsay Cedex, France

[d]*INFN - Sezione di Pavia,*
 Via Bassi 6, 27100 Pavia, Italy

[e]*Theory Unit, Physics Department, CERN,*
 Geneva 23, Switzerland

 E-mail: c.carloni-calame@phys.soton.ac.uk, stefano@phys.soton.ac.uk,
 fulvio.piccinini@cern.ch, dar@phys.soton.ac.uk

ABSTRACT: We describe the impact of the full one-loop EW terms of $\mathcal{O}(\alpha_S \alpha_{EM}^3)$ entering the electron-positron into three-jet cross-section from $\sqrt{s} = M_Z$ to TeV scale energies. We include both factorisable and non-factorisable virtual corrections, photon bremsstrahlung but not the real emission of $W^{\pm}$ and Z bosons. Their importance for the measurement of α_S from jet rates and shape variables is explained.

Contents

1 Introduction

Strong (QCD) and Electro-Weak (EW) interactions are two fundamental forces of Nature, the latter in turn unifying Electro-Magnetic (EM) and Weak (W) interactions in the Standard Model (SM). A clear hierarchy exists between the strength of these two interactions at the energy scales probed by past and present high energy particle accelerators (e.g., LEP, SLC, HERA and Tevatron): QCD forces are stronger than EW ones. This is quantitatively manifest if one recalls that the value of the QCD coupling, α_S, measured at these machines is much larger than the EM one, α_{EM}, typically, by an order of magnitude. This argument, however, is only valid in lowest order in perturbation theory.

A peculiar feature distinguishing QCD and EW effects in higher orders is that the latter are enhanced by (Sudakov) double logarithmic factors, $\ln^2(\frac{s}{M_W^2})$, which, unlike in the former, do not cancel for 'infrared-safe' observables [1–4]. The origin of these 'double logs' is well understood. It is due to a lack of the Kinoshita-Lee-Nauenberg (KLN) [5] type cancellations of Infra-Red (IR) — both soft and collinear — virtual and real emission in higher order contributions originating from $W^\pm$ (and, possibly, Z: see Footnote 1) exchange. This is in turn a consequence of the violation of the Bloch-Nordsieck theorem [6] in non-Abelian theories [7]. The problem is in principle present also in QCD. In practice, however, it has no observable consequences, because of the final averaging of the colour degrees of freedom of partons, forced by their confinement into colourless hadrons. This does not occur in the EW case, where the initial state has a non-Abelian charge, dictated by the given collider beam configuration, such as in e^+e^- collisions.

These logarithmic corrections are finite (unlike in QCD), as the masses of the weak gauge bosons provide a physical cut-off for $W^\pm$ and Z emission. Hence, for typical experimental resolutions, softly and collinearly emitted weak bosons need not be included in the production cross-section and one can restrict oneself to the calculation of weak effects

originating from virtual corrections and affecting a purely hadronic final state.[1] Besides, these contributions can be isolated in a gauge-invariant manner from EM effects [3], at least in some specific cases, and therefore may or may not be included in the calculation, depending on the observable being studied. As for purely EM effects, since the (infinite) IR real photon emission cannot be resolved experimentally, this ought to be combined with the (also infinite) virtual one, through the same order, to recover a finite result, which is however not doubly logarithmically enhanced (as QED is an Abelian theory).

In view of all this, it becomes of crucial importance to assess the quantitative relevance of such EW corrections affecting, in particular, key QCD processes studied at past, present and future colliders, such as $e^+e^- \to 3$ jets.

2   Three-jet events at leptonic colliders

It is the aim of our paper to report on the computation of the full one-loop EW effects entering three-jet production in electron-positron annihilation at any collider energy via the subprocesses $e^+e^- \to \gamma^*, Z \to \bar{q}qg$.[2] Ref. [10, 45] tackled part of these, in fact, restricted to the case of $W^\pm$ and Z (but not γ) exchange and when the higher order effects arise only from initial or final state interactions (these represent the so-called 'factorisable' corrections, i.e., those involving loops not connecting the initial leptons to the final quarks or gluons, which are the dominant ones at $\sqrt{s} = M_Z$, where the width of the Z resonance provides a natural cut-off for off-shellness effects). The remainder, 'non-factorisable' corrections, while being typically small at $\sqrt{s} = M_Z$, are expected to play a quantitatively relevant role as $\sqrt{s}$ grows larger. Since, here, we study the full set the one-loop EW corrections, we improve on the results of ref. [10, 45] in two respects:

  (i) we include now all the non-factorisable terms;

  (ii) we also incorporate previously neglected genuine QED corrections, including photon bremsstrahlung.

In contrast, we refrain here from computing $W^\pm$ and Z boson bremsstrahlung (just like in [10, 45]), as we will argue that this may not enter the experimental jet samples. (For a study of the impact of the emission of real massive gauge bosons in a variety of high energy processes, see ref. [11], albeit in hadronic collision.)

Combining the aforementioned logarithmic enhancement associated with the genuinely weak component of the EW corrections to the fact that α_S steadily decreases with energy, unlike α_{EW}, in general, one expects one-loop EW effects to become comparable to QCD ones at future Linear Colliders (LCs) [12] running at TeV energy scales, like those available at an International Linear Collider (ILC) or the Compact LInear Collider (CLIC).[3] In

---

[1]By doing so, double logarithms also arise from virtual Z exchange, despite there being no flavour change, simply because KLN cancellations are spoilt by the remotion of real Z emission.

[2]See ref. [8] for the corresponding one-loop corrections to the Born process $e^+e^- \to q\bar{q}$ and ref. [9] for the $\sim n_f$ component of those to $e^+e^- \to q\bar{q}gg$ (where n_f represents the number of light flavours).

[3]For example, at one-loop level, in the case of the inclusive cross-section of e^+e^- into hadrons, the QCD corrections are of $\mathcal{O}(\frac{\alpha_S}{\pi})$, whereas the EW ones are of $\mathcal{O}(\frac{\alpha_{EW}}{4\pi} \ln^2 \frac{s}{M_W^2})$, where s is the collider centre-of-mass (CM) energy squared, so that at $\sqrt{s} \approx 1.5\,\text{TeV}$ the former are identical to the latter, of order 9% or so.
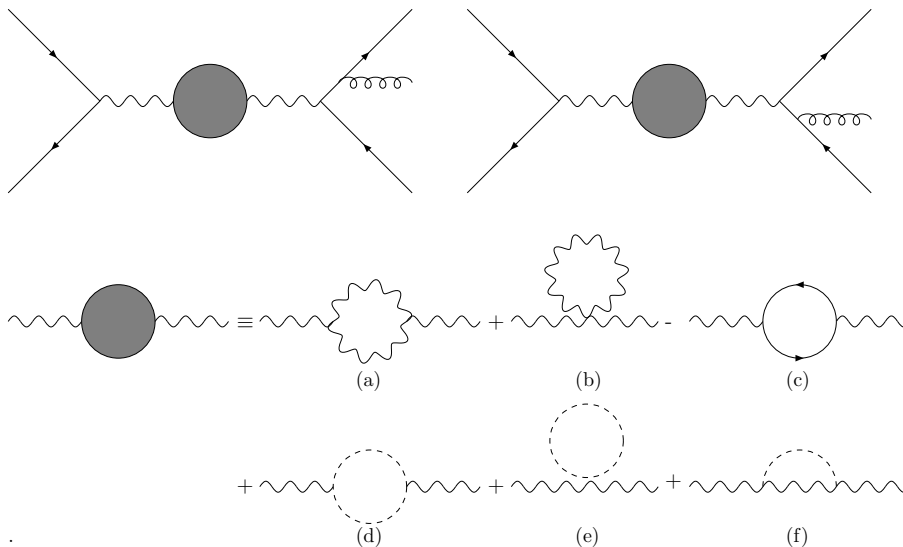
Figure 1. Internal and external bosonic self-energy graphs. The shaded blob on the wavy lines represents all the contributions to the gauge boson self-energy and is dependent on the Higgs mass, as detailed in the graphical equation. These corrections apply to the photon self-energy, the Z boson self-energy and the photon-Z mixing. The gauge bosons inside the loops are $W^\pm$ and the scalars are charged Goldstone bosons. In the case of the self-energy of the Z, in graphs (d)–(f), the gauge boson inside the loop can be a Z and the scalar a Higgs boson.

contrast, at the Z mass peak, where logarithmic enhancements are not effective, one-loop EW corrections are expected to appear at the percent level, hence being of limited relevance at LEP1 and SLC, where the final error on α_S is of the same order or larger [13], but of crucial importance at a GigaZ stage of a future LC [10, 45], where the relative accuracy of α_S measurements is expected to be at the 0.1% level or better [14]. On the subject of higher order QCD effects, it should be mentioned here that a great deal of effort has recently been devoted to evaluate two-loop contributions to the three-jet process [15] while the one-loop QCD results have been known for quite some time [16].

As intimated, in the case of e^+e^- annihilations, the most important QCD quantity to be extracted from multi-jet events is α_S. The confrontation of the measured value of the strong coupling constant with that predicted by the theory through the renormalisation group evolution is an important test of the SM. Alternatively, it may be an indication of new physics, when its typical mass scale is larger than the collider energy, so that the new particles cannot be produced as 'real' detectable states but may manifest themselves through 'virtual' effects. Not only jet rates, but also jet shape observables would be affected.

The calculation we are presenting here involves the full one-loop EW corrections to three-jet observables in electron-positron annihilations generated via the interference of the graphs in figures 1–6 with the tree-level ones for $e^+e^- \rightarrow \gamma^*, Z \rightarrow \bar{q}qg$. Hence, our calculation not only accounts for the aforementioned double logarithms, but also all single ones as well as the finite terms arising through the complete $\mathcal{O}(\alpha_S \alpha_{\mathrm{EW}}^3)$. We will account for all possible flavours of (anti)quarks in the final state, with the exception of the top quark.
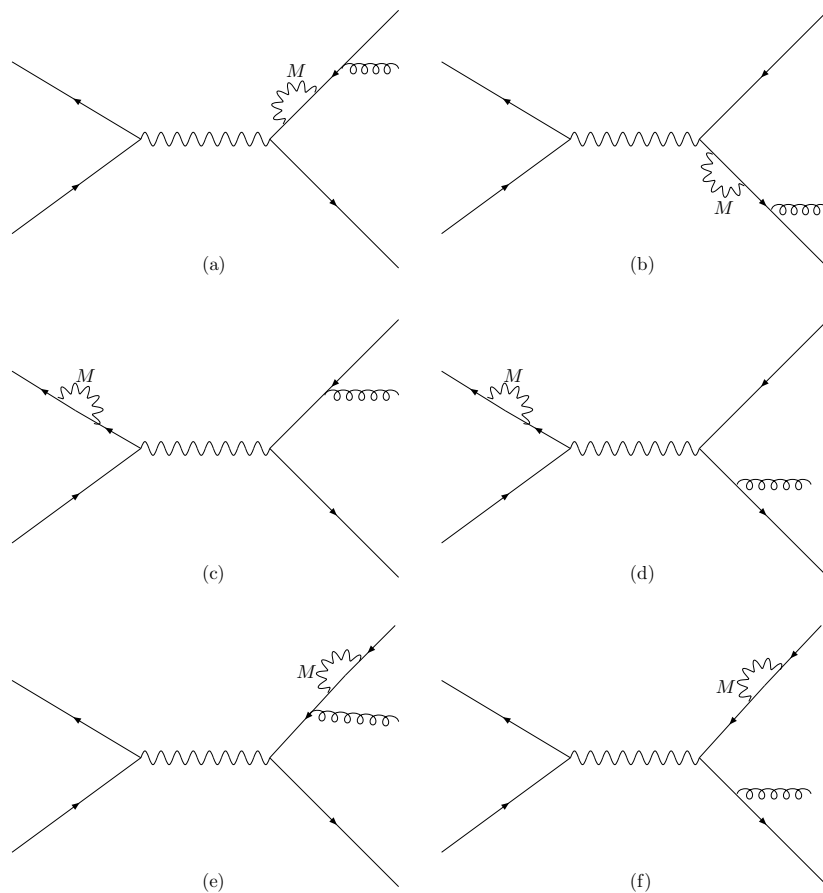
Figure 2. Internal and external fermionic self-energy graphs. The gauge boson mass, M, can take the values λ, M_Z or M_W. For the external self-energies, we display only the self-energy insertion on the incoming positron (c), (d) or outgoing antiquark (e), (f). There is an identical contribution from self-energy insertions on the electron or quark, but each carries a combinatorial factor of $\frac{1}{2}$.

The latter however appears in some of the loops whenever a $b\bar{b}g$ final state is considered.

We will show that all such corrections can range from a few percent to a few tens of percent, both at $\sqrt{s} = M_Z$ and LC energies, depending on the observable under study, with the QED component being preponderant at low energy and the weak one emerging more and more as the latter increases. Altogether, while their impact is not dramatic in the context of LEP1 and SLC physics at a GigaZ stage of future LCs they ought to be taken into account in the experimental fits. This is even more the case of future LCs running at and beyond the TeV range.[4]

---

[4]Another relevant phenomenological aspect of our calculation would pertain to the case in which the bremsstrahlung photon is resolved, so that a three-jet plus one-photon sample can be defined and compared to a four-jet sample in order to extract genuine non-Abelian QCD effects, as detailed in [17] — and references therein – but we postpone this analysis to a future work.
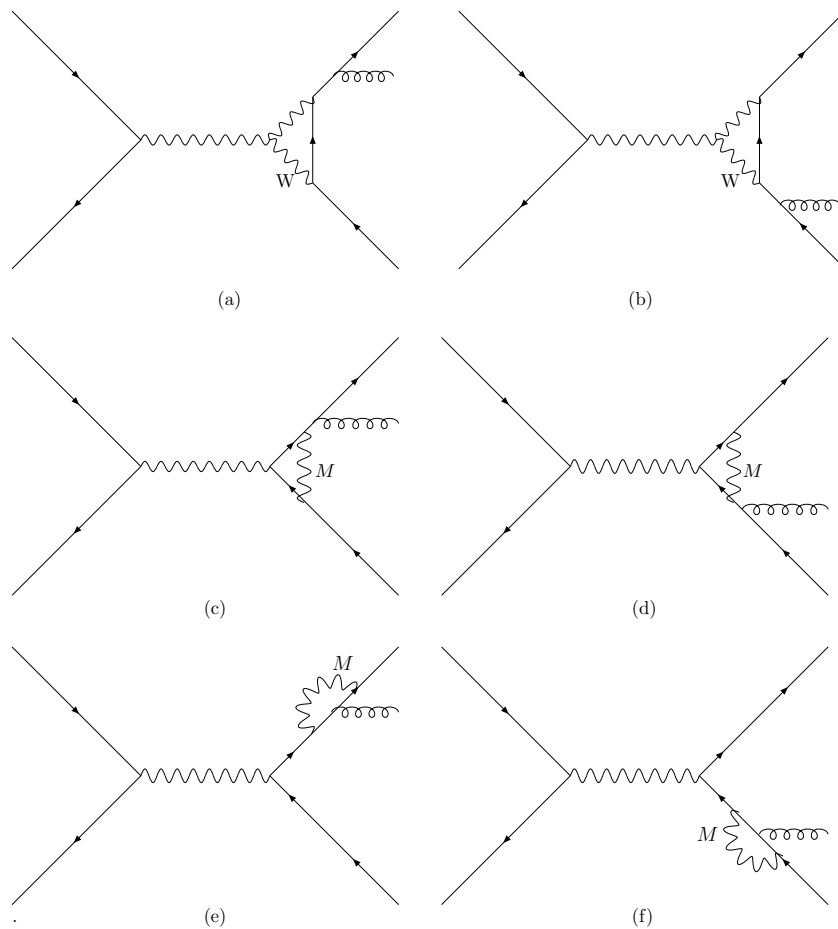
Figure 3. Vertex graphs. Corrections on the (anti)quark line. In graphs (a) and (b) the gauge boson mass inside the loop must be M_W whereas for graphs (c) to (f) the gauge boson mass M can take the values λ, M_Z or M_W.

The plan of the rest of the paper is as follows. In the next section, we describe the calculation. Then, in section 4, we present some numerical results (a preliminary account of which was given in ref. [18]). We conclude in section 5.

3 Calculation

In ref. [45], which concentrated only on the factorisable corrections to three-jet production (i.e., neglecting any interaction between the incoming electron-positron pair and the final-state (anti)quarks), the method of helicity Matrix Elements (MEs) was adopted. In the present case such an approach is not convenient because we have to address the problem of IR divergent contributions from loops in which a photon is exchanged. As intimated already, this means that we also need to consider the real photon (bremsstrahlung) contributions, summed over the helicities of the emitted photon. Moreover, since in our numerical simulations, as we will see later, we regularise the collinear singularities with finite fermion masses, the introduction of these terms would complicate the expressions
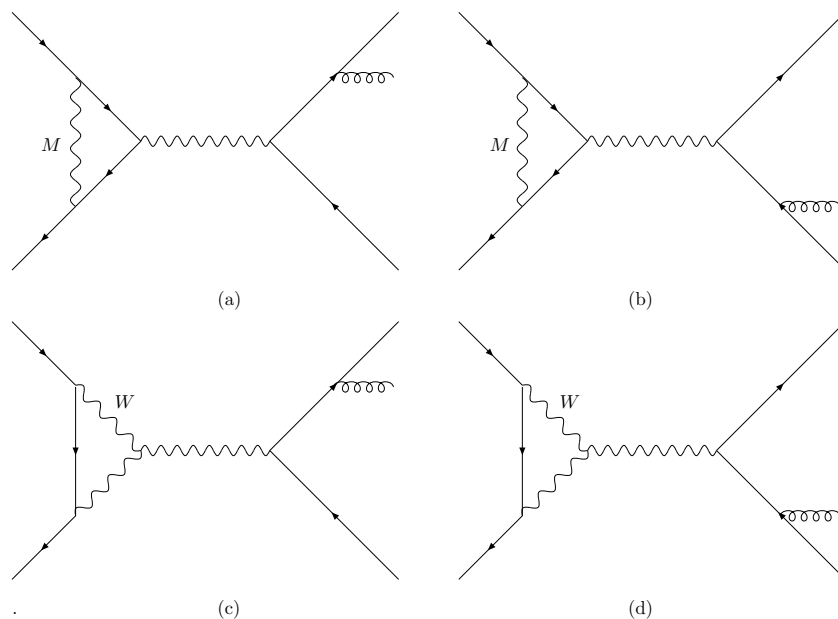
Figure 4. Vertex graphs. Corrections on the electron/positron line. In graphs (a) and (b) the gauge boson mass mass M can take the values λ, M_Z or M_W whereas in graphs (c) and (d) inside the loop there must be M_W.

obtained within the helicity formalism. For the virtual corrections, we therefore adopt the more traditional approach of considering all possible interferences between the one-loop and tree-level graphs.[5] We have organized the former into "prototype graphs", shown in figures 1–6, which were calculated as general functions of couplings and internal masses, which appear inside Passarino-Veltman (PV) functions [19], which are then determined numerically with the appropriate couplings and internal masses. In doing so, we have made extensive use of the FORM [20] program.

In anticipation of an electron-positron collider in which the incoming beams can be polarised, we have however inserted a helicity projection operator into the electron line and obtained separate results for left-handed and right-handed incoming electrons.[6] For genuinely weak interaction corrections, this is of particular interest, since such corrections violate parity conservation. Unfortunately, this occurs already at tree-level, owing to the contribution from exchange of a Z boson, but these higher order corrections are also peculiarly dependent on the incoming lepton helicity and thus one would expect the two parity-violating effects be distinguishable after the collection of sufficient events. (We will devote a separate paper to the study of polarised incoming beams.)

In this connection, it is worth mentioning that as we are dealing with weak interactions, which involve axial couplings, and as we furthermore wish to distinguish between left- and

---

[5]We have however verified that, limitedly to the case of factorisable corrections, we can reproduce the (unpolarised) results of ref. [10, 45].

[6]As we are taking massless incoming fermions, the helicity of the positron is simply the opposite to that of the electron.
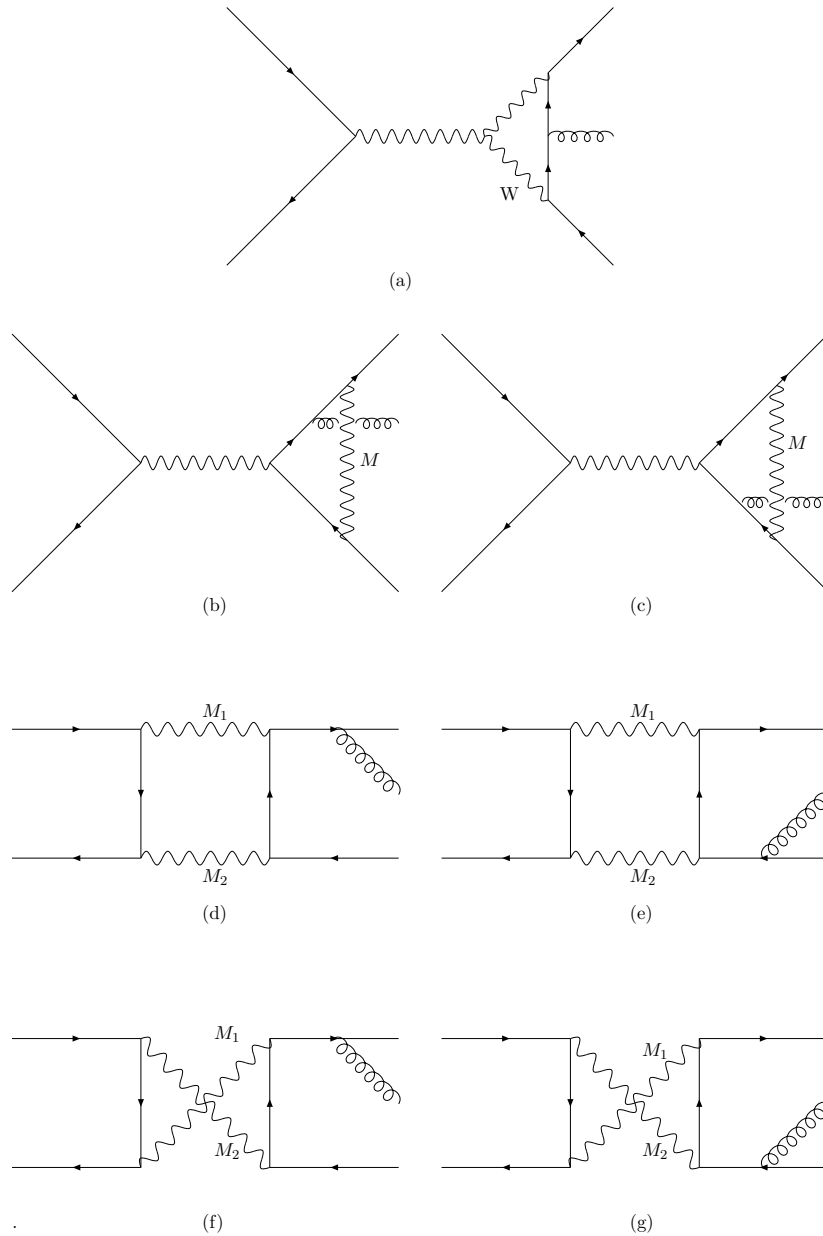
Figure 5. Box graphs. In the non-factorising corrections (d)–(f), the gauge boson masses M_1, M_2 can each take the values λ or M_Z or they can both be M_W.

right-helicity incoming electrons, the only unambiguous way to handle loop integrals is to use the 'modified' Dimensional Reduction ($\overline{\text{DR}}$) as opposed to the 'modified' Minimal Subtraction ($\overline{\text{MS}}$) renormalisation prescription. (We use $\mu = M_Z$ as the subtraction scale of ultraviolet divergences.) It is therefore necessary to determine the value of the fine-structure constant α_{EM} in that scheme at the subtraction point $\mu = M_Z$.[7] For the light

---

[7]We emphasise that we are *not* using the complex mass subtraction scheme of ref. [21], but rather the $\overline{\text{DR}}$ one in which all counterterms are taken to be real. For the internal gauge boson self-energies the mass
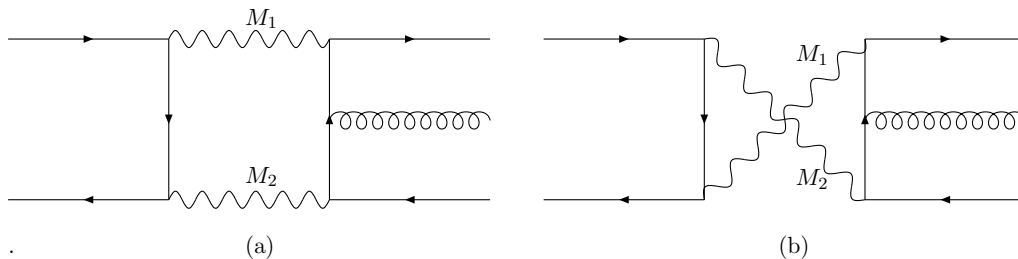
Figure 6. Pentagon graphs. The gauge boson masses can take the same values as in the case of the non-factorising box graphs.

fermion (including the b-quark) contributions we can integrate the β-function through the thresholds at $Q^2 = 4m_i^2$, for all charged fermions with mass $2m_i < M_Z$. There is a difficulty here with the light quarks as one expects substantial QCD corrections and the mass thresholds are well below the regime where perturbative QCD is reliable. This problem is usually addressed by considering the total cross-section for electron-positron annihilation in the resonant region and applying a finite energy sum rule. This has been carried out in detail in ref. [22]. The upshot of this numerical analysis is that the effect of all light fermions can be simulated by using ordinary perturbation theory with a threshold of $15\,\mathrm{MeV}$ for the u- and d-quarks and $1\,\mathrm{GeV}$ for the s-quark, yielding a value $\alpha_{\mathrm{EM}}^{\mathrm{MOM}}(M_Z^2) = 1/128.2$, in the MOMentum (MOM) subtraction renormalisation scheme. However, there is a finite difference between this prescription and a genuine $\overline{\mathrm{DR}}$ determination arising from:

1. contributions to the photon self-energy from loops of $W^\pm$ gauge bosons (and their attendant Goldstone bosons);

2. a contribution from the non-vanishing Z photon mixing part of the self-energy at zero momentum;

3. a contribution from the loop correction to the EM vertex involving internal $W^\pm$'s, which does *not* cancel by virtue of the QED Ward identity, owing to the non-Abelian nature of the coupling of the photon to charged gauge bosons.

These corrections have been considered in ref. [23] in the $\overline{\mathrm{MS}}$ scheme. In the $\overline{\mathrm{DR}}$ scheme we find that these give a total contribution of

$$\Delta\left(\alpha_{\mathrm{EM}}^{\overline{\mathrm{DR}}}(M_Z^2)\right) \;=\; -\frac{7\alpha_{\mathrm{EM}}^2(M_Z^2)}{4\pi}\ln\left(\frac{M_W^2}{M_Z^2}\right), \tag{3.1}$$

subtraction is the on-shell self-energy. Provided this is taken in conjunction with the corresponding values for the EM coupling, α_{EM}, and the weak mixing angle, θ_W (as discussed here), this is an equally consistent scheme in which the imaginary parts of the renormalised couplings in the scheme of [21] are reproduced by the imaginary parts of the subtracted gauge boson self-energies.

where s_W and c_W are $\sin\theta_W$ and $\cos\theta_W$, respectively. This introduces a negligible correction.

Finally, we need to account for the difference between the MOM and the $\overline{\text{DR}}$ schemes, from the light fermions (including the b-quark), and a contribution from the t-quark, which lead to the more substantial corrections

$$\Delta\left(\alpha_{\text{EM}}^{\overline{\text{DR}}}(M_Z^2)\right) \;=\; \frac{\alpha_{\text{EM}}^2(M_Z^2)}{3\pi}\left[\sum_i q_i^2 \ln(4) - \frac{4}{3}\ln\left(\frac{m_t^2}{M_Z^2}\right)\right], \tag{3.2}$$

where the sum is over all fermions whose electric charge is $q_i\,e$, except the t-quark. This gives us a final value of

$$\alpha_{\text{EM}}^{\overline{\text{DR}}}(M_Z^2) \;=\; \frac{1}{127.7}. \tag{3.3}$$

Loops containing one or two photons give rise to IR divergences. For all of these divergent loop integrals we have a means of isolating the IR part in the $\overline{\text{DR}}$ scheme in $4-2\epsilon$ dimensions. This is explained in detail in the appendix. For *all* of these IR divergent integrals we have checked numerically that the introduction of a common mass, λ, for *both* the internal fermion lines and the internal photon lines reproduces these integrals upon the replacements

$$\pi^{-\epsilon}\Gamma(\epsilon) \;\to\; \ln(\lambda^2),$$
$$\pi^{-\epsilon}\frac{\Gamma(\epsilon)}{\epsilon} \;\to\; \frac{1}{2}\ln^2(\lambda^2),$$

provided λ is chosen sufficiently small, but not so small as to introduce numerical instabilities. In each case we have identified a substantial plateau region in λ where the two methods of calculation agree to a very high degree of accuracy.

Having established that this works, we then abandon the use of dimensional regularisation for the case of IR divergences and simply insert a mass regulator λ for the photon and an independent mass m_f for all fermions. This is also done in the case of the bremsstrahlung contribution before integrating over the phase space for the emitted photon. The reason why the mass regularisation of IR (i.e., soft/collinear) singularities works is linked to the fact that the tree-level diagrams only involve neutral currents, so that the EM and purely weak corrections are separately gauge invariant, as mass regularisation is well known to work in QED. By varying both of these parameters and noting the insensitivity of the final results to these changes, we have checked the expected cancellations of these divergences between the virtual correction and real emission.

A new feature of this calculation, which was not present in the case of factorisable corrections only dealt with in [45], is the occurrence of pentagon graphs, as shown in figure 6, which arise from interactions with two gauge bosons exchanged in the s-channel and the gluon emitted from an internal (anti)quark. Such graphs involve five-point PV functions with up to three powers of momenta in the numerator. We have handled these in two separate ways (with two independently developed codes), in order to check for possible numerical instabilities. In the first case the integrals are simply evaluated using routines in `LoopTools v2.2` [24], for which these tensor-type pentagon integrals are now implemented

according to the reduction formalism of ref. [25].[8] In the other we use the standard PV reduction to express scalar products of the loop momentum k with external momenta p_i in terms of the denominators of propagators adjacent to the i-th vertex. This reduction is carried out exhaustively until only scalar pentagon integrals appear. The latter are available in the library FF1.9 [26]. A comparison of the numerical results provided by the two codes for a sample of phase space points yielded satisfactory agreement between the two methods.

The square MEs and the interferences for the bremsstrahlung process have been calculated directly using ALPHA [27] and checked against both MadGraph [28] and the results based on the codes of ref. [29], finding perfect agreement between all these implementations.

Regarding the integration over the photon phase space, this has been split into two regions

1. $E_\gamma \leq \Delta E$.

2. $E_\gamma > \Delta E$.

For the first region, the MEs have been approximated using the eikonal approximation in which a fermion with momentum p emitting a photon (with polarisation ϵ) has an associated vertex $2p \cdot \epsilon$ and the photon momentum is neglected in all numerators. Here, the phase space integration has been performed analytically assuming a photon mass λ. In the second region, the full MEs are employed but the photon mass is set to zero. Here, we integrate over *all* the phase space available to the photon. The integrations for both the three- and four-particle final states were performed numerically with Monte Carlo (MC) techniques, so that any desired cut on the final state can be imposed.

The three- and four-particle Lorentz invariant phase space reads as

$$d^5\Phi_3 = \frac{1}{8(2\pi)^5} \frac{d^3\mathbf{p}_q}{E_q} \frac{d^3\mathbf{p}_{\bar{q}}}{E_{\bar{q}}} \frac{d^3\mathbf{p}_g}{E_g} \, \delta^4(p_{e^+} + p_{e^-} - p_q - p_{\bar{q}} - p_g),$$

$$d^8\Phi_4 = \frac{1}{16(2\pi)^8} \frac{d^3\mathbf{p}_q}{E_q} \frac{d^3\mathbf{p}_{\bar{q}}}{E_{\bar{q}}} \frac{d^3\mathbf{p}_g}{E_g} \frac{d^3\mathbf{p}_\gamma}{E_\gamma} \, \delta^4(p_{e^+} + p_{e^-} - p_q - p_{\bar{q}} - p_g - p_\gamma), \qquad (3.4)$$

respectively. We choose as five (eight) independent integration variables for the three (four) body phase space the angles of the quark, the energy and the angles of the gluon (and the energy and the angles of the photon). With this choice, eq. (3.4) can be written as

$$d^5\Phi_3 = \frac{1}{8(2\pi)^5} \frac{|\mathbf{p_q}|E_g}{|E_{\bar{q}} + E_q\left(1 + \mathbf{p}_g \cdot \mathbf{p}_q/|\mathbf{p}_q|^2\right)|} dE_g d^2\Omega_g d^2\Omega_q,$$

$$d^8\Phi_4 = \frac{1}{16(2\pi)^8} \frac{|\mathbf{p_q}|E_g E_\gamma}{|E_{\bar{q}} + E_q\left[1 + (\mathbf{p}_g + \mathbf{p}_\gamma) \cdot \mathbf{p}_q/|\mathbf{p}_q|^2\right]|} dE_g d^2\Omega_g dE_\gamma d^2\Omega_\gamma d^2\Omega_q. \qquad (3.5)$$

In eq. (3.5), all the kinematical quantities are derived from the independent variables by imposing four-momentum conservation and mass-shell relations and are calculated in the rest frame of the incoming e^+e^- system.

---

[8]We implemented also directly in an independent FORTRAN routine the expressions for the five-point functions of ref. [25], finding agreement with LoopTools up to available digits precision.

λ^2 (GeV^2)	$5 \cdot 10^{-10}$	$1 \cdot 10^{-13}$
$\sigma_V + \sigma_S$ (pb), $\sqrt{s} = 90\,\mathrm{GeV}$	-4181.6 ± 5	-4181.2 ± 5
$\sigma_V + \sigma_S$ (pb), $\sqrt{s} = 350\,\mathrm{GeV}$	-1.2293 ± 0.005	-1.2293 ± 0.005

Table 1. Variation of the soft plus virtual cross section $\sigma_V + \sigma_S$ for two different values of λ for $\sqrt{s} = 90$ and $350\,\mathrm{GeV}$. Here, only order α_{EM} QED contributions are included, the cuts are specified in the text and $2\Delta E/\sqrt{s}$ is 10^{-4}. The sum over the final-state quark flavours is taken.

$2\Delta E/\sqrt{s}$	10^{-3}	10^{-4}
σ_{real} (pb), $\sqrt{s} = 90\,\mathrm{GeV}$	$5054. \pm 1.$	$5050. \pm 2$
σ_{real} (pb), $\sqrt{s} = 350\,\mathrm{GeV}$	1.978 ± 0.001	1.979 ± 0.001

Table 2. Variation of the four-body cross section σ_{real} for two different values of ΔE, wherein λ^2 is fixed to the value $10^{-13}\,\mathrm{GeV}^2$. Again, only order α_{EM} QED contributions are included, $\sqrt{s}$ is 90 and $350\,\mathrm{GeV}$, the cuts are specified in the text and the sum over the final-state quark flavours is taken.

In order to perform the numerical integration over the phase space, the independent variables are sampled according to the peaking structure of the integrand function. Standard multi-channel importance sampling techniques are used. Concerning the importance sampling of the three- and four-body phase space collinear configurations, our treatment closely follows the multi-channel approach described in appendix A.3 of ref. [30].

As intimated, we have checked that the final result is insensitive to variations of (small values) of not only the fictitious photon mass λ but also the separator ΔE. Table 1 shows the sum of the virtual, σ_V, and soft, σ_S, cross section (integrated on E_γ from λ to ΔE), while spanning a wide range of values for λ. Table 2 shows the real radiation cross section, σ_{real}, where the integration on E_γ is split in the soft part $\lambda \leq E_\gamma \leq \Delta E$ and the hard part $\Delta E \leq E_\gamma \leq E_\gamma^{\mathrm{max}}$. (Parameters and cuts on the hadronic system are defined in the following section.)

When the real photon emission process is combined with the virtual corrections we have checked that the limit $\lambda \to 0$ may be taken, whilst keeping the fermion mass m_f small but non-zero. The collinear divergence obtained when $m_f \to 0$ cancels with the well-known exception of an overall large logarithm $(\ln(s/m_f^2))$, which is associated with the Initial State Radiation (ISR) induced by the incoming electrons and positrons.

It is well known that, in the case of QCD, such a remnant collinear divergence is absorbed into the momentum dependence of the Parton Distribution Functions (PDFs). In the case of electron-positron colliders this large correction is always present, but it is universal to all processes and would therefore tend to mask the purely weak corrections. However, for sensible numerical results, it has to be accounted for to all orders of perturbation theory, e.g., within the so-called electron/positron structure function formalism [31], which automatically resums in QED all Leading Logarithmic (LL) terms. In ref. [32] a method of combining consistently resummed LL calculations with exact $\mathcal{O}(\alpha_{\mathrm{EM}})$ ones has

been devised both in additive and factorisable form. Here, we will adopt the additive approach, which amounts to write the differential cross section as

$$d\sigma = d\sigma_{\mathrm{LL}} - d\sigma_{\mathrm{LL}}^{\alpha} + d\sigma_{\mathrm{exact}}^{\alpha}, \tag{3.6}$$

where $d\sigma_{\mathrm{LL}}$ and $d\sigma_{\mathrm{LL}}^{\alpha}$ are defined by

$$d\sigma_{\mathrm{LL}} = \int dx_1 dx_2 D(x_1, s) D(x_2, s) d\sigma_0(x_1 x_2 s),$$

$$d\sigma_{\mathrm{LL}}^{\alpha} = \int dx_1 dx_2 [D(x_1, s) D(x_2, s)]_{\alpha} d\sigma_0(x_1 x_2 s) \tag{3.7}$$

and where $D(x, Q^2)$ is the electron structure function whilst $[D(x_1, s)D(x_2, s)]_{\alpha}$ is the order α_{EM} term of $D(x_1, s)D(x_2, s)$. In eq. (3.6), the order α_{EM} part of the up-to-all-order resummed cross section in LL approximation is replaced by the exact order α_{EM} correction or, in other words, the higher-order (beyond order α_{EM}) LL corrections are added to the exact order α_{EM} calculation.

There remains one kinematic region where our results would not be numerically reliable. In the case of real photon emission, the aforementioned ISR can lead to the situation in which the remaining sub-energy of the incoming electron-positron pair is close the the Z mass and hence close to the pole of the propagator in the case of Z boson s-channel exchange. In order to avoid this the width, Γ_Z, of the Z boson has been included in the propagator. For consistency, this means that the same width has to be included in the Z propagator for the virtual corrections. This can be done in a consistent way in the $\overline{\mathrm{DR}}$ scheme used in this paper, in which renormalised couplings remain real, as well as the the complex mass scheme [21], where the W and Z masses are defined as the locations of the propagator poles in the complex plane, and the couplings become complex. The essential ingredient for the evaluation of virtual corrections is the ability to compute one-loop integrals with complex internal masses. The package `LoopTools v2.2` [24] implements complex masses only for two-point, three-point and IR-singular four-point functions. We implemented in `LoopTools` the general expression for the scalar four-point function of ref. [33], valid also for complex masses. Particular attention has been devoted to the occurrence of numerical instabilities in certain regions of phase space because of strong cancellations. The new routine for the scalar four-point function with complex masses has been tested with extended `complex*32` precision, finding perfect numerical agreement. Actually, for the present study, the implementation of the complex mass scheme is only partial since we have kept real couplings and thus our scheme is equivalent to the fixed width scheme [34] implemented at the full one-loop level. In principle this could produce a bad high energy behaviour of the corrections. We tested the stability of our predictions at high energy by switching off the W/Z width in the virtual and real corrections, checking that the effect of the width is smaller and smaller as the energy raises up to 1 TeV: the differences on the pure virtual corrections with and without W/Z width (and setting $\lambda^2 = 5 \cdot 10^{-10}\,\mathrm{GeV}^2$) are 0.5% at $\sqrt{s} = 350\,\mathrm{GeV}$, 0.2% at $\sqrt{s} = 700\,\mathrm{GeV}$ and 0.1% at $\sqrt{s} = 1\,\mathrm{TeV}$, in units of the Born cross section.

We have neglected the masses of light quarks throughout. However, in the case in which the final state contains a $b\bar{b}$ pair, whenever there is a $W^{\pm}$ boson in the virtual loops,

account had to be taken of the mass of the top (anti)quark. Furthermore, in such cases, it was also necessary to supplement the graphs shown in figures 1–6 with the corresponding diagrams in which one or two internal $W^\pm$ bosons are replaced by charged Goldstone bosons, as appropriate. Having done all this, we are therefore in a position to present the results for such 'b-jets' separately, though this will also be done in another publication.

4   Numerical results

Before proceeding to show our results, we should mention the parameters we set for our simulations. We have taken the top (anti)quark to have a mass $m_t = 171.6\,\text{GeV}$. The Z mass used was $M_Z = 91.18\,\text{GeV}$ and was related to the $W^\pm$ mass, M_W, via the SM formula $M_W = M_Z \cos\theta_W$, where $\sin^2\theta_W = 0.222478$. The Z width was $\Gamma_Z = 2.5\,\text{GeV}$. Also notice that, where relevant, Higgs contributions are included with $M_H = 115\,\text{GeV}$. For the strong coupling constant, α_S, we have used the two-loop expression with $\Lambda_{\text{QCD}}^{(nf=4)} = 0.325\,\text{GeV}$ in the $\overline{\text{MS}}$ scheme, yielding $\alpha_\text{S}^{\overline{\text{MS}}}(M_Z^2) = 0.118$.

All the numerical results presented in this section are obtained considering a realistic experimental setup. Namely, partonic momenta are clustered into jets according to the Cambridge jet algorithm [35] (e.g., when $y_{ij} < y_\text{cut}$ with $y_\text{cut} = 0.001$), the jets are required to lie in the central detector region $30° < \theta_\text{jets} < 150°$ and we request that the invariant mass of the jet system M_{3j} is larger than $0.75 \times \sqrt{s}$. If a real photon is present in the final state, it is clustered according to the same algorithm, but we require that at least three "hadronic" jets are left at the end (i.e., events in which the photon is resolved are rejected). Notice that this procedure serves a twofold purpose. On the one hand, from the experimental viewpoint, a resolved (energetic and isolated) single photon is never treated as a jet. On the other hand, from a theoretical viewpoint, this enables us to remove divergent contributions appearing whenever an unresolved real gluon is produced via an IR emission, as we are not computing here $\mathcal{O}(\alpha_\text{S}\alpha_\text{EM}^3)$ one-loop QCD corrections to $e^+e^- \to q\bar{q}\gamma$. Finally, we sum over the final-state quarks. In order to show the behaviour of the corrections we are calculating, other than scanning in the collider energy, we have considered here the three discrete values of $\sqrt{s} = M_Z\,\text{GeV}$, $\sqrt{s} = 350\,\text{GeV}$ and $\sqrt{s} = 1\,\text{TeV}$.

In figure 7, the relative effects[9] on the cross section (integrated within the experimental cuts defined above) induced by different contributions to the order $\alpha_\text{S}\alpha_\text{EM}^3$ correction are plotted as a function of the CM energy, in the range from $150\,\text{GeV}$ to $1\,\text{TeV}$. The curves represent the effect of the QED (virtual and real) corrections only, the effect of the gauge bosons self-energy corrections (given by the graphs of figure 1), the effect of the non-factorisable graphs of figures 5 (d)–(f) and 6 with WW exchange,[10] the effect of the weak corrections with the non-factorizing WW graphs removed (labelled as "full weak - non-fact WW graphs") and the total effect as the sum of the previous ones: the total effect is increasingly negative, reaching the -13% level at $1\,\text{TeV}$. It is worth mentioning that, as far as the non-factorisable WW corrections (represented by the graphs in figures 5 (d)–(f) and 6) are

---

[9]The effects are relative to the lowest-order cross section.
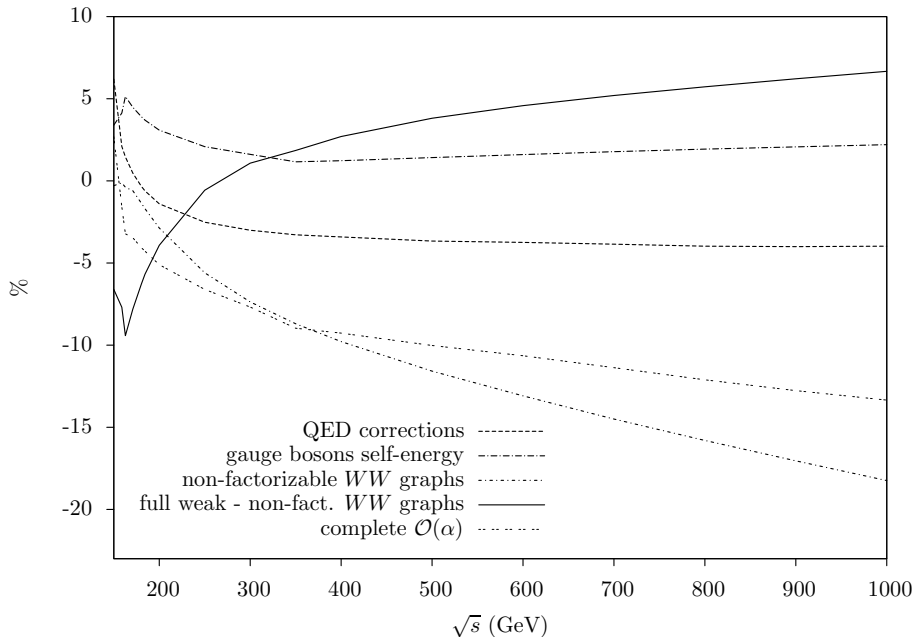[10]This is a gauge invariant subset of the complete correction.

Figure 7. Relative effect on the integrated cross section due to different contributions to the order $\alpha \equiv \alpha_{\rm EM}$ correction, as a function of the CM energy. For setup and input parameters, see the text.

concerned, in the case of d, s and b final-state quarks, only the direct diagrams (figure 5 (d)–(e) and figure 6 (a)) are present due to charge conservation, while, for u and c quarks, only crossed diagrams are present, if the sum over initial- and final-state helicities is taken. In the case of ZZ exchange, all the graphs survive, giving rise to a cancellation at the leading-log level between direct and crossed diagrams, which does not occurr for WW exchange. Hence, the big negative correction is due to the presence of the WW non-factorisable graphs, which develop the aforementioned large Sudakov double logarithms in the high energy regime.

We then show the impact of the EW corrections on some differential distributions of phenomenological interest. We organize the plots by showing the tree-level contributions and the higher order corrections in three different contributions: the purely weak-interaction contribution (labelled "weak $\mathcal{O}(\alpha)$"), purely weak plus QED corrections, which are dominated by the above-mentioned ISR (labelled "exact $\mathcal{O}(\alpha)$"), and the weak plus electromagnetic correction in which the leading logarithms have been summed (labelled "exact $\mathcal{O}(\alpha)$ + h.o.LL"). The figures show in the upper panel the absolute distributions and in the lower panel the relative differences with respect to the tree-level rates. In figure 8, the azimuthal angle of the leading jet[11] distribution is shown at the Z peak. Here, the largest contribution to the total correction (-30% or so) comes from QED ISR because of the radiative return phenomenon. The purely weak corrections are negative and at the level of $3-4\%$. The higher-order QED radiation tends to compensate the order $\alpha_{\rm EM}$ effect, since it enhances the cross section by $\sim 5\%$. By raising the CM energy, the relative weight of the weak corrections becomes more important (see figures 9 and 10 for the leading jet

---
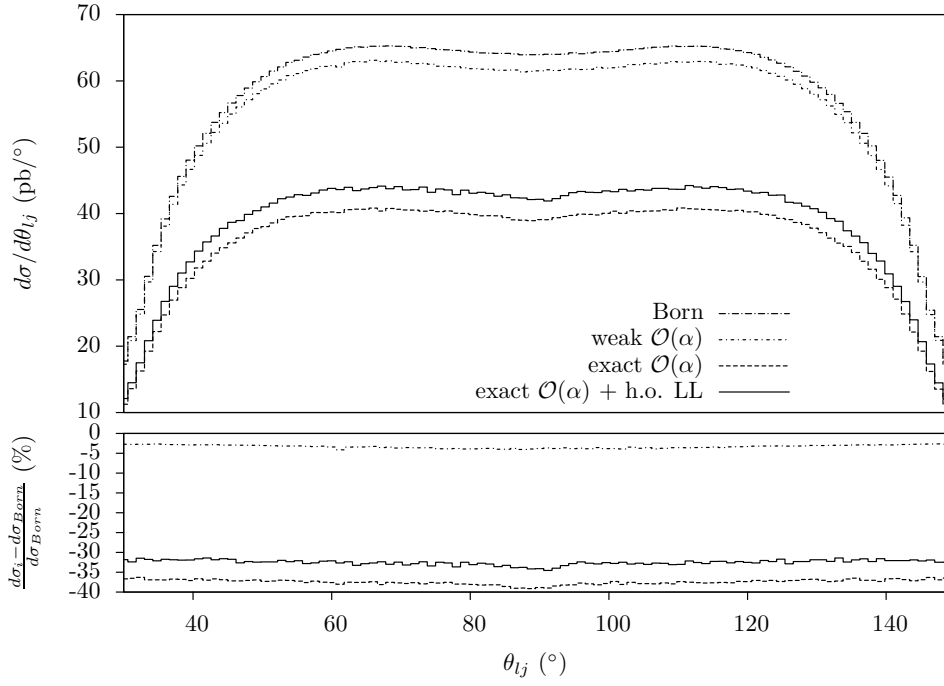
[11]The leading jet is defined as the most energetic one.
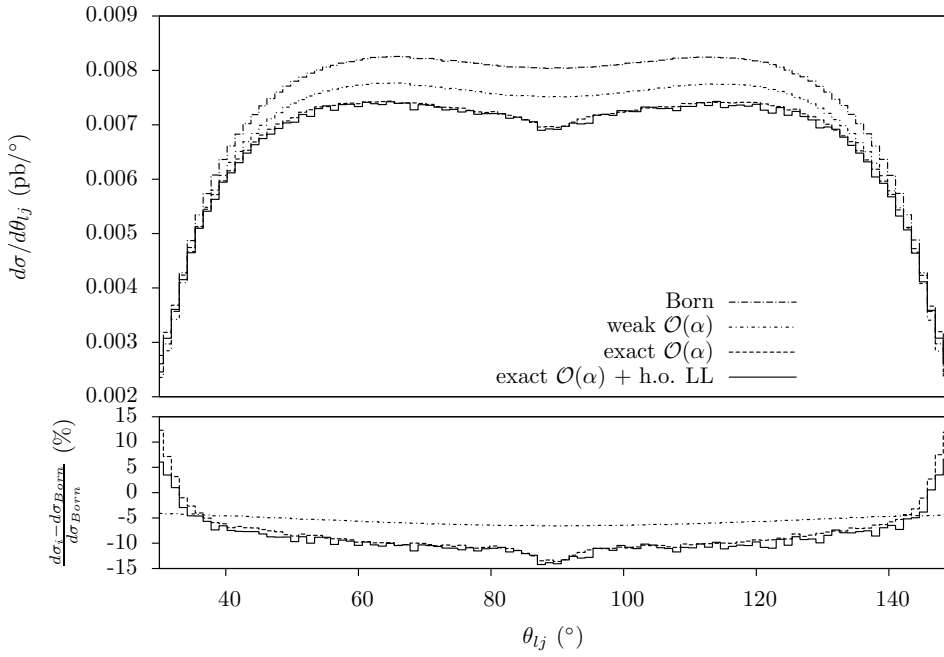
Figure 8. Leading jet angle distribution at the Z peak.

Figure 9. Leading jet angle distribution at $350\,\mathrm{GeV}$.

angle distribution at $\sqrt{s} = 350\,\mathrm{GeV}$ and $1\,\mathrm{TeV}$, respectively) and the effect of higher-order QED corrections becomes negligible. It is worth noticing that, far from the Z peak, the cut $M_{3j} > 0.75 \times \sqrt{s}$ is more effective in reducing the radiative return phenomenon, reducing
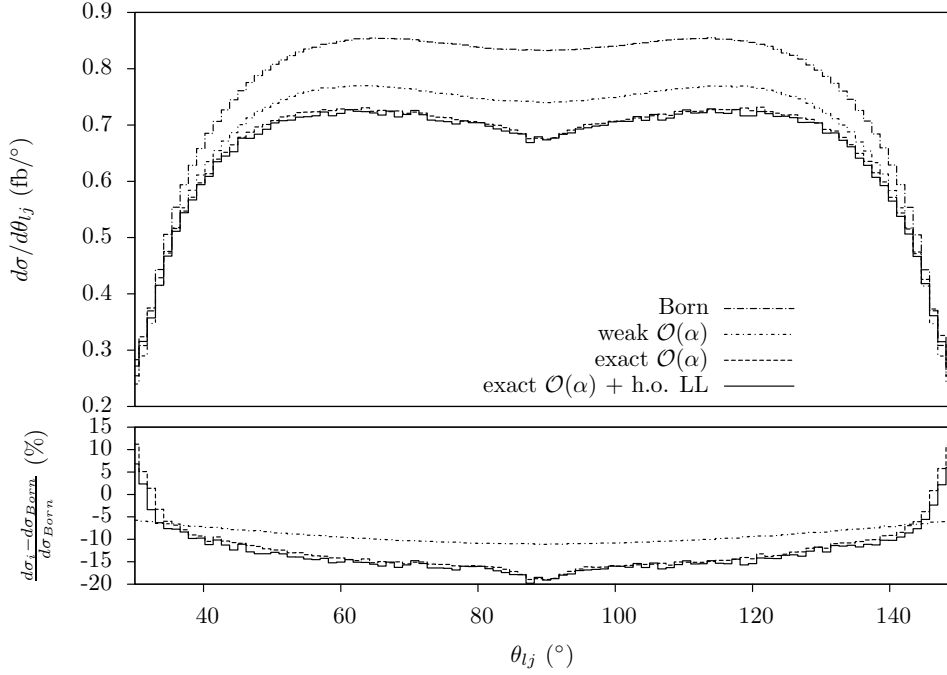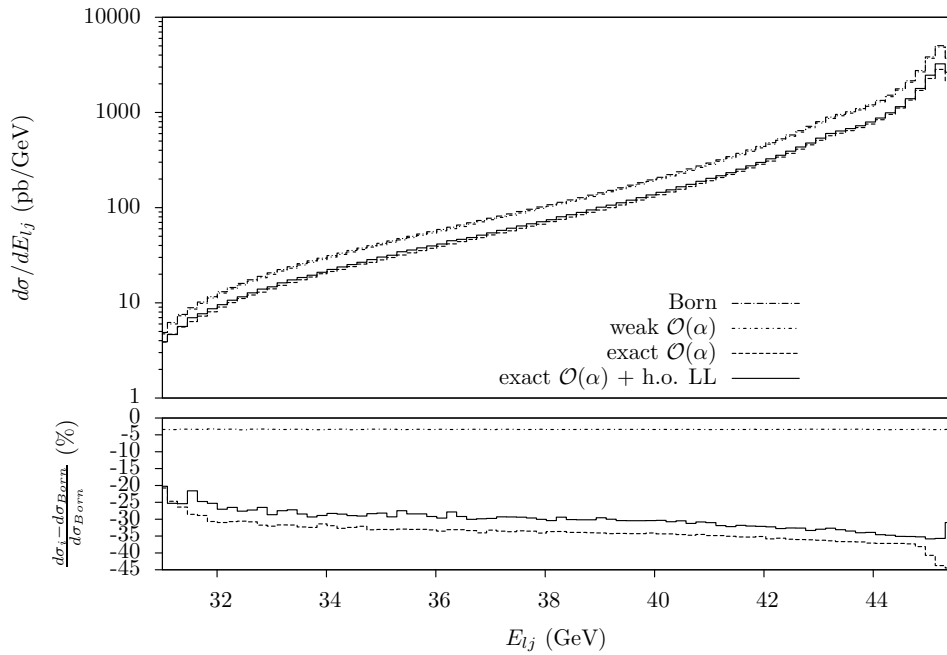
Figure 10. Leading jet angle distribution at 1 TeV.

Figure 11. Leading jet energy distribution at the Z peak.

in turn the relative effect of ISR.

In figures 11, 12 and 13 the leading jet energy is presented at $\sqrt{s} = M_Z$, 350 GeV and 1 TeV. This distribution is much more sensitive to the real radiation, as it can be expected. The corrections are very large in the distribution tail, where however the cross
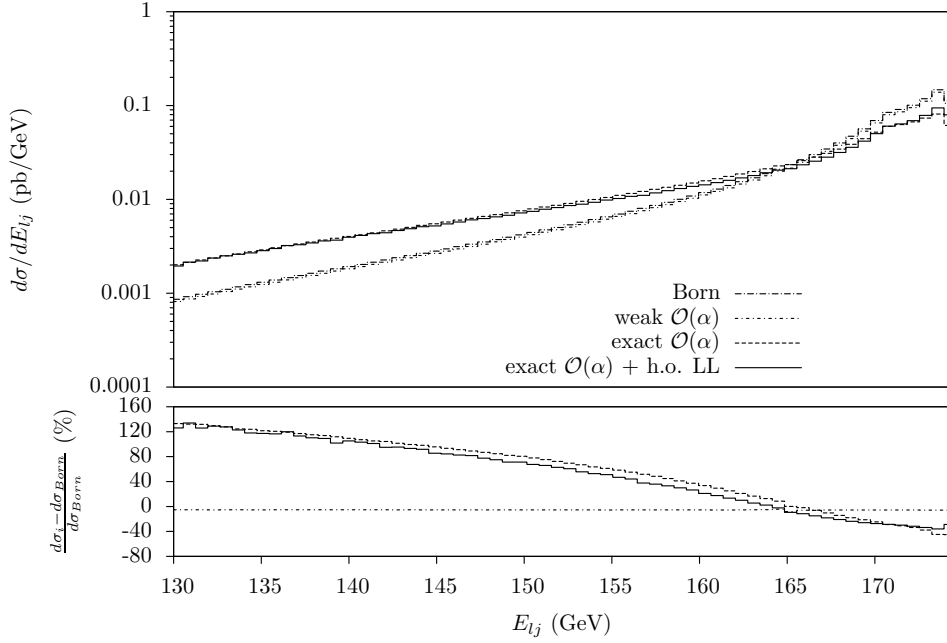
Figure 12. Leading jet energy distribution at $350\,\mathrm{GeV}$.
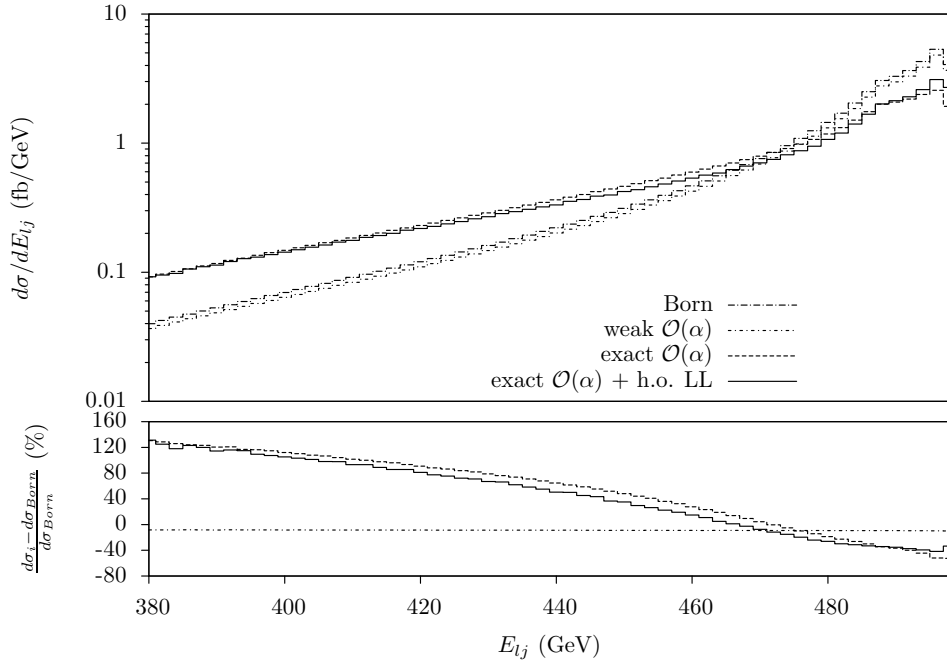
Figure 13. Leading jet energy distribution at $1\,\mathrm{TeV}$.

section is small.

In the following some event shape variables are considered: the *thrust* T [36], the *spherocity* S [37], the C-parameter [38] and the *oblateness* O [39]. One should notice that, owning to the fact that — as intimated — we are not computing here $\mathcal{O}(\alpha_S \alpha_{\mathrm{EM}}^3)$
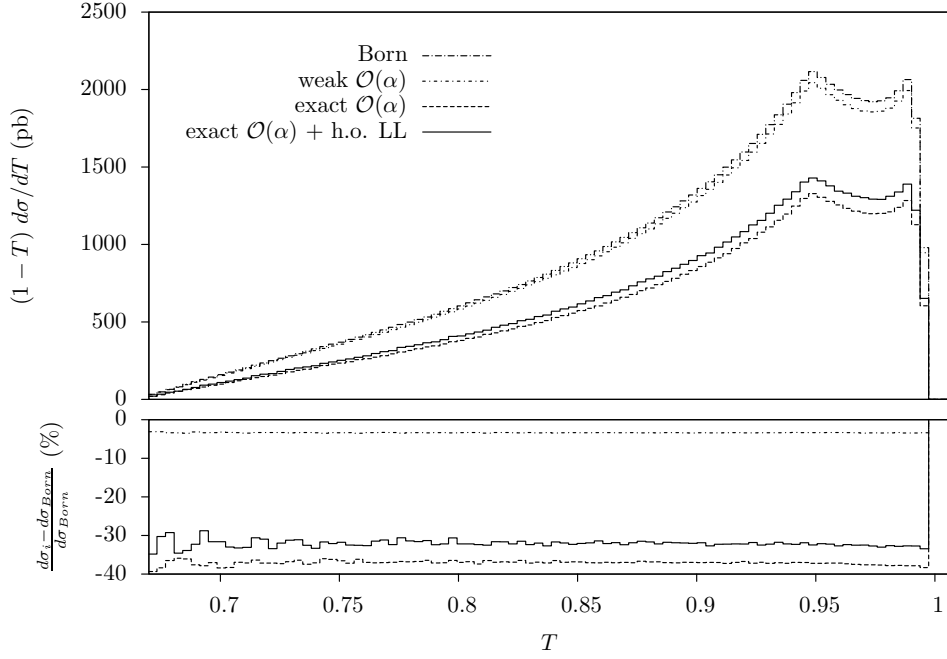
Figure 14. $(1-T)\frac{d\sigma}{dT}$ distribution at the Z peak.
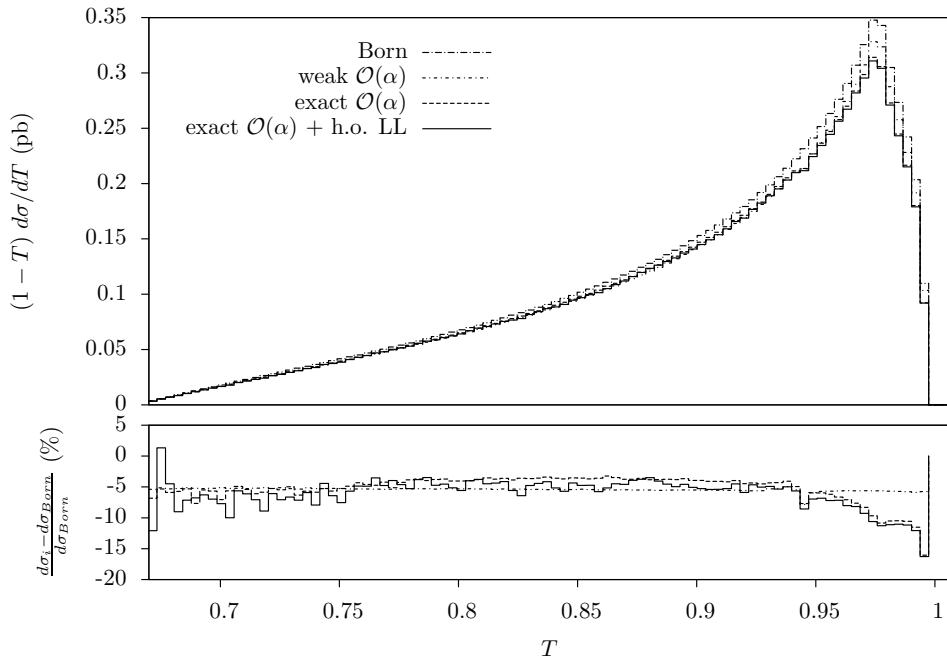
Figure 15. $(1-T)\frac{d\sigma}{dT}$ distribution at $350\,\text{GeV}$.

one-loop QCD corrections to $q\bar{q}\gamma$ final states necessary to remove singularities associated with IR real gluon emission from $q\bar{q}g\gamma$ ones, we ought to maintain a y_{cut} between jets (we use our default value), thereby defining the shape variables using the jets three-momenta, which at the same time enables us to remove energetic and isolated 'photon jets' from the
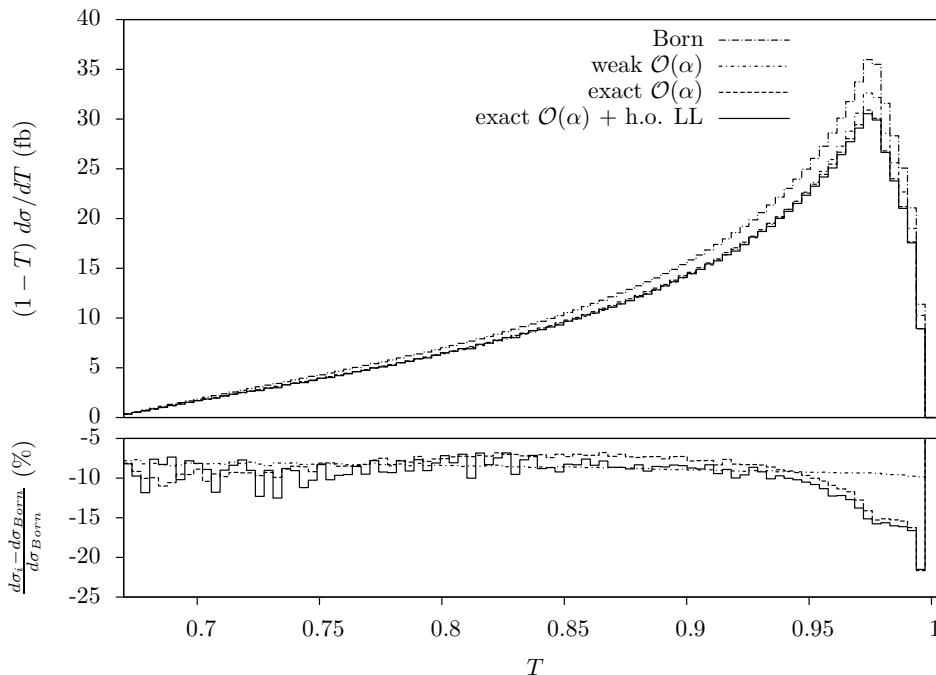
Figure 16. $(1-T)\frac{d\sigma}{dT}$ distribution at $1\,\mathrm{TeV}$.

final state. (In fact, for consistency, 'photon jets' are not used in the calculation of the shape variables even when the gluon is resolved in a $q\bar{q}g\gamma$ final state.) This is not unlike typical experimental procedures, whereby resolved photons from either the ISR or from the final state (i.e., those not originating from parton fragmentation) are separated from the hadronic system by using a jet clustering algorithm.[12] In figures 14, 15 and 16, the distribution $(1-T)\frac{d\sigma}{dT}$ is shown. T is defined as

$$T = \max_{\vec{n}}\frac{\sum_i |\vec{p_i}\cdot\vec{n}|}{\sum_i |\vec{p_i}|},\tag{4.1}$$

where the sum runs over the reconstructed jet momenta and $\vec{n}$ is the thrust axis. The T distribution is one of the key observables used for the measurement of α_{S} in e^+e^- collisions [41]. It is worth noticing that while the purely weak corrections give an almost constant effect on the whole T range, the presence of the real bremsstrahlung gives a non trivial effect in the region $T > 0.92$. In view of a precise measurement of α_{S} at a future LC, EW corrections can play an important role.

In figures 17, 18 and 19, the distribution $\frac{d\sigma}{dS}$ is shown. S is defined as

$$S = \left(\frac{4}{\pi}\right)^2 \min_{\vec{n}}\frac{\sum_i |\vec{p_i}\times\vec{n}|}{\sum_i |\vec{p_i}|},\tag{4.2}$$

where the sum runs over the reconstructed jet momenta and $\vec{n}$ is the spherocity axis. The effect of pure weak corrections is flat over the whole S range increasing in size from few
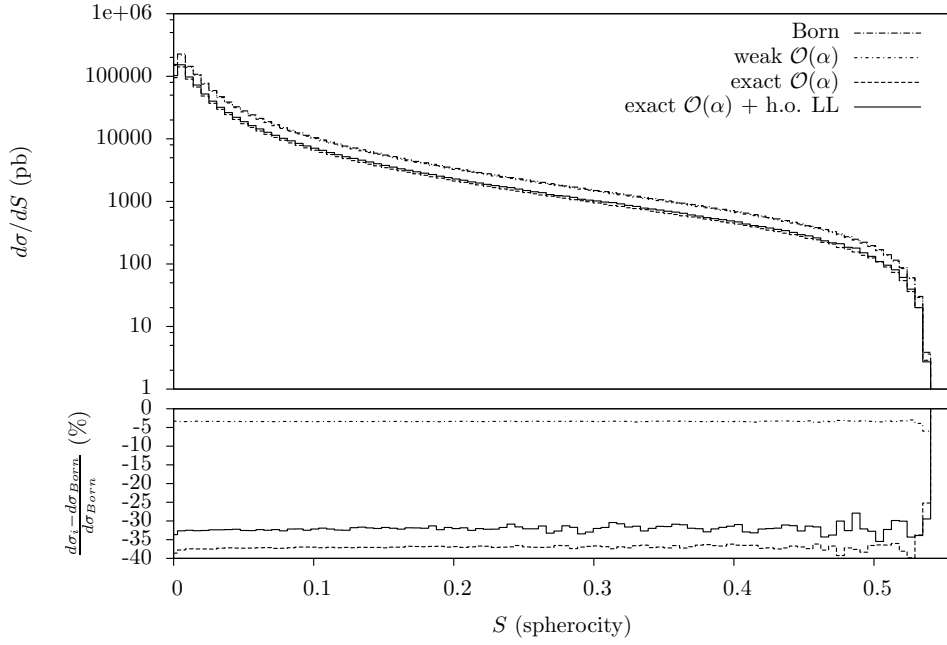

Figure 17. $\frac{d\sigma}{dS}$ distribution at the Z peak.
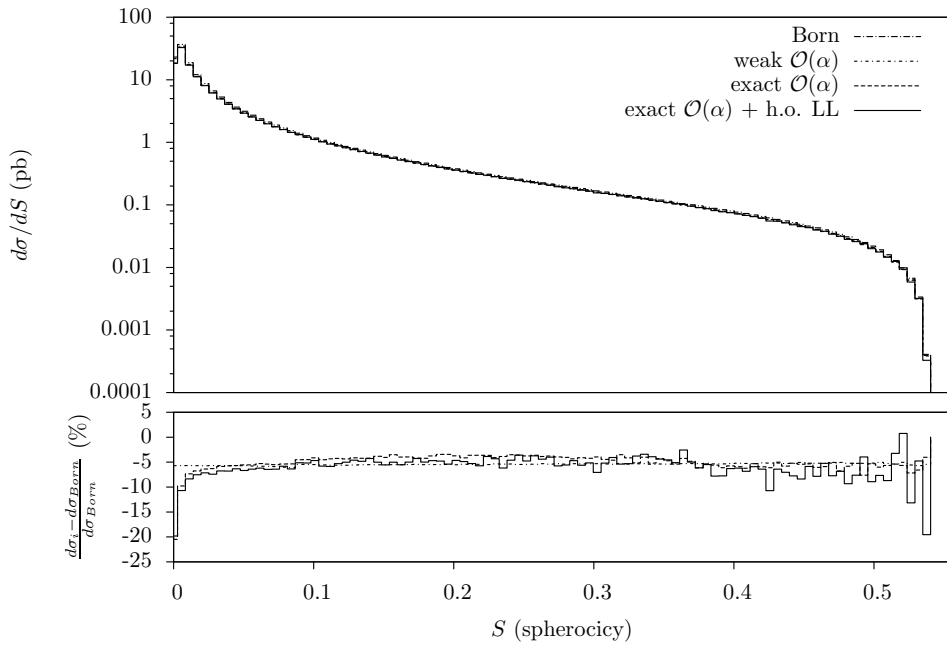
Figure 18. $\frac{d\sigma}{dS}$ distribution at $350\,\text{GeV}$.

percent at the Z peak to about 10% at $1\,\text{TeV}$. The addition of QED radiation at $\mathcal{O}(\alpha)$ and at all orders does not change the picture except for the Z peak, where the $\mathcal{O}(\alpha)$ contribution is about 30% and the higher order corrections give an additional 10% effect.
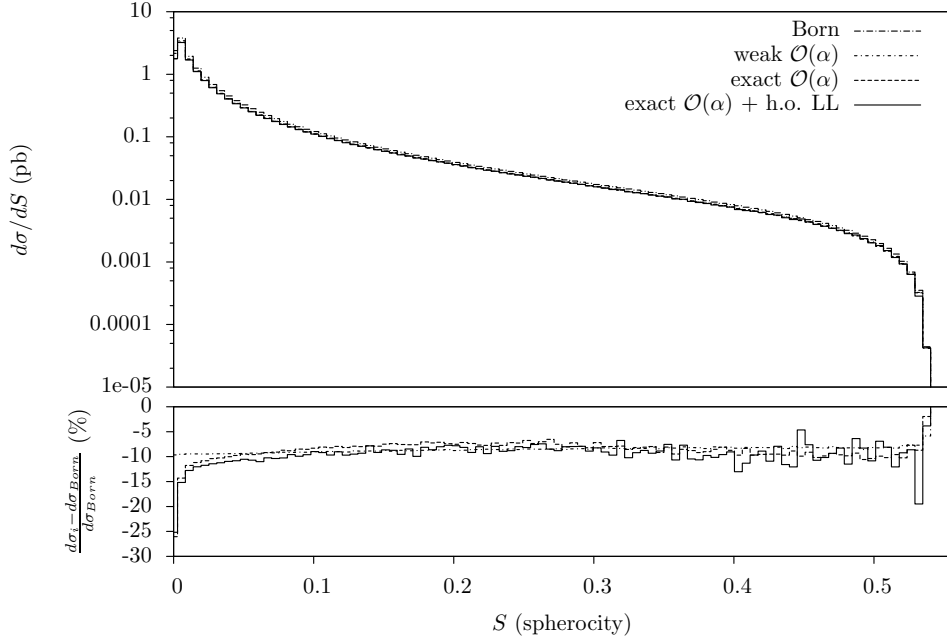
Figure 19. $\frac{d\sigma}{dS}$ distribution at 1 TeV.
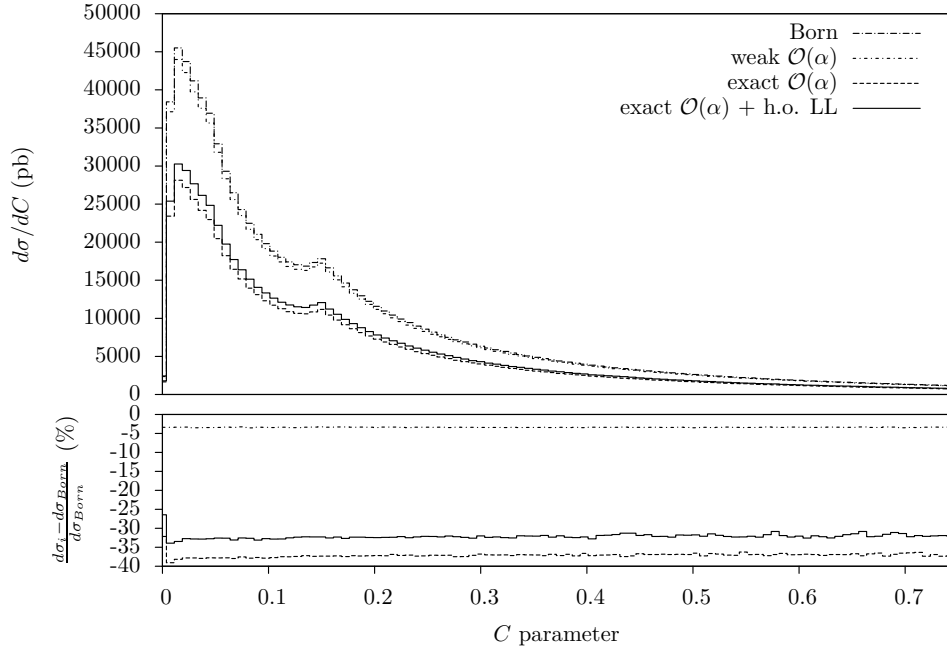
Figure 20. $\frac{d\sigma}{dC}$ distribution at the Z peak.

In figures 20, 21 and 22, the distribution $\frac{d\sigma}{dC}$ is shown. C is defined as

$$C = \frac{3}{2} \frac{\sum_{i,j} [|\vec{p_i}||\vec{p_j}| - (\vec{p_i} \cdot \vec{p_j})^2/|\vec{p_i}||\vec{p_j}|]}{(\sum_i |\vec{p_i}|)^2}, \tag{4.3}$$

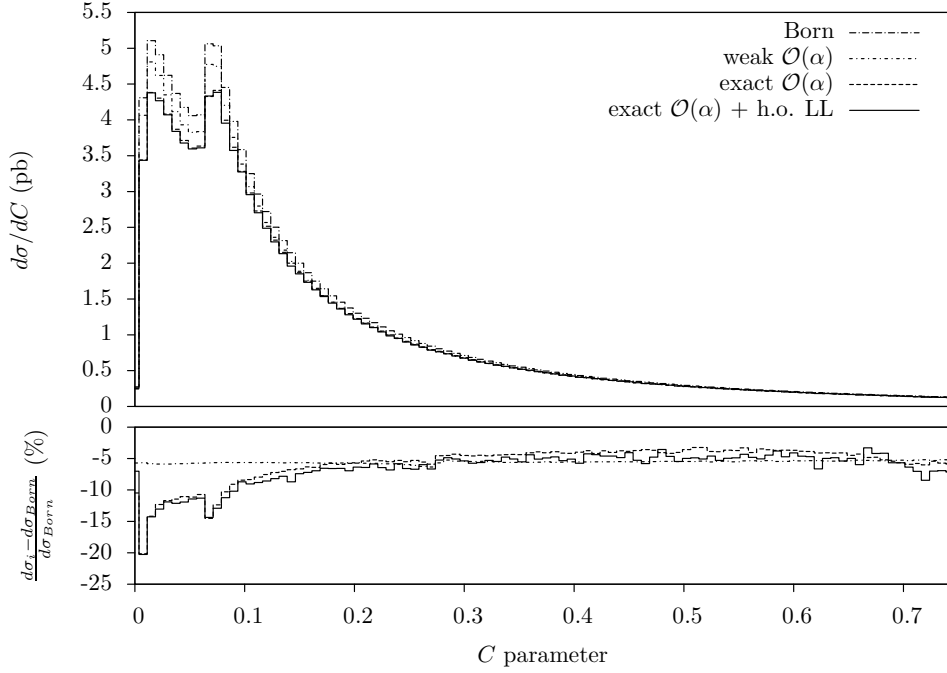where the sum runs over the reconstructed jet momenta. The effect of pure weak corrections

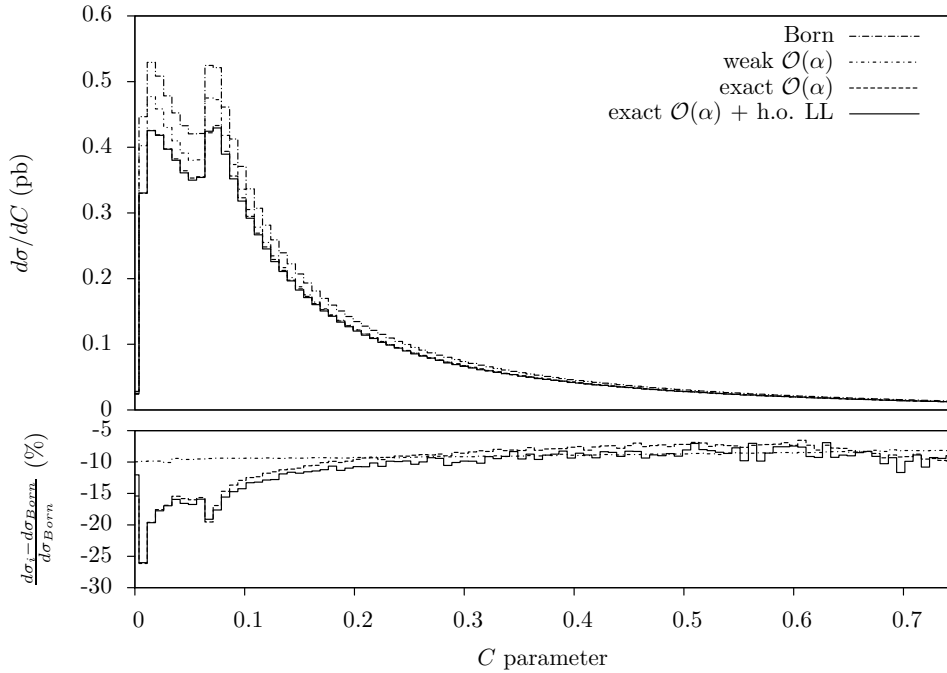**Figure 21**. $\frac{d\sigma}{dC}$ distribution at $350\,\mathrm{GeV}$.

Figure 22. $\frac{d\sigma}{dC}$ distribution at $1\,\mathrm{TeV}$.

is similar in magnitude and shape to the case of spherocity and thrust. The addition of QED radiation is very large only at the Z peak ($\sim 30\%$) while for higher energies it introduces a non trivial shape in the region $C \lesssim 0.15$.
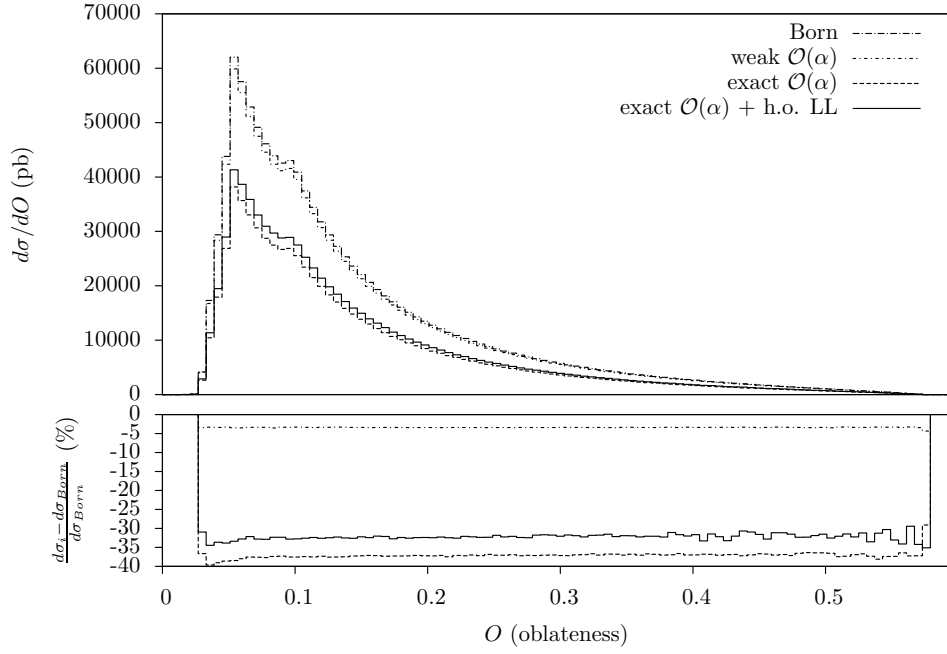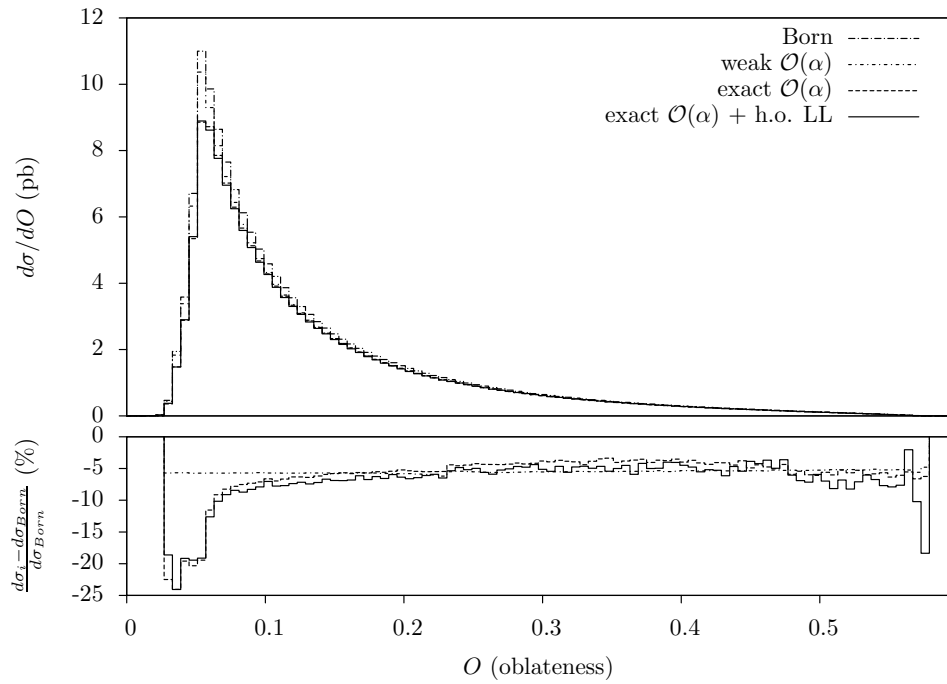
Figure 23. $\frac{d\sigma}{dO}$ distribution at the Z peak.

Figure 24. $\frac{d\sigma}{dO}$ distribution at $350\,\mathrm{GeV}$.

In figures 23, 24 and 25, the distribution $\frac{d\sigma}{dO}$ is shown. O is defined as
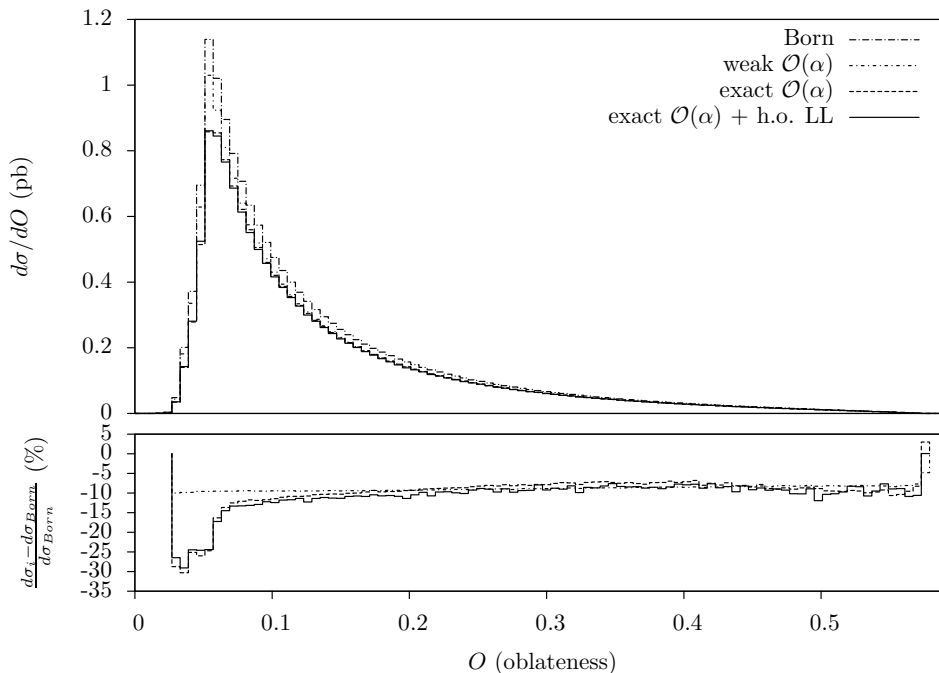
$$O = F_{\mathrm{major}} - F_{\mathrm{minor}}\,,$$

Figure 25. $\frac{d\sigma}{dO}$ distribution at 1 TeV.

$$F_{\mathrm{major}} = \frac{\sum_i |\vec{p}_i \cdot \vec{n}_{\mathrm{major}}|}{\sum_i |\vec{p}_i|},$$
$$F_{\mathrm{minor}} = \frac{\sum_i |\vec{p}_i \cdot \vec{n}_{\mathrm{minor}}|}{\sum_i |\vec{p}_i|}, \tag{4.4}$$

where $\vec{n}_{\mathrm{major}}$ is an axis which lyes in the plane perpendicular to the thrust axis and the magnitude of the momenta projected into this plane is maximal along this axis; $\vec{n}_{\mathrm{minor}}$ is orthogonal to the thrust axis and $\vec{n}_{\mathrm{major}}$. The numerical impact of the various contributions is similar to the case of the C-parameter. The region where QED real radiation introduces non trivial effects is $C \lesssim 0.1$.

In figures 26, 27 and 28 the y distribution is shown. For each event, the observable y is defined as the minimum (Cambridge) y_{ij} such as $y_{ij} > y_{\mathrm{cut}} = 0.001$. Also on this distribution the weak effects are quite constant, while real radiation distorts its shape. Finally, figures 29, 30 and 31 represent the cross sections integrated over y in the range $y_{\mathrm{cut}} < y < y_{\mathrm{max}}$, as a function of y_{max}. Corrections can be very large in both distributions generally at any energy, reaching the several tens of percent.

5 Conclusions

In summary, we have shown the phenomenological relevance that the calculation up to $\mathcal{O}(\alpha_{\mathrm{S}}\alpha_{\mathrm{EW}}^3)$ can have in the study of (unflavoured) three-jet samples in e^+e^- annihilation, for all energies ranging from $\sqrt{s} = M_Z$ to 1 TeV. Not only inclusive jet rates are affected, but also more exclusive distributions, both global (like the event shape variables) and individual (like energy and angles) ones. Effects range from a few percent to several tens of
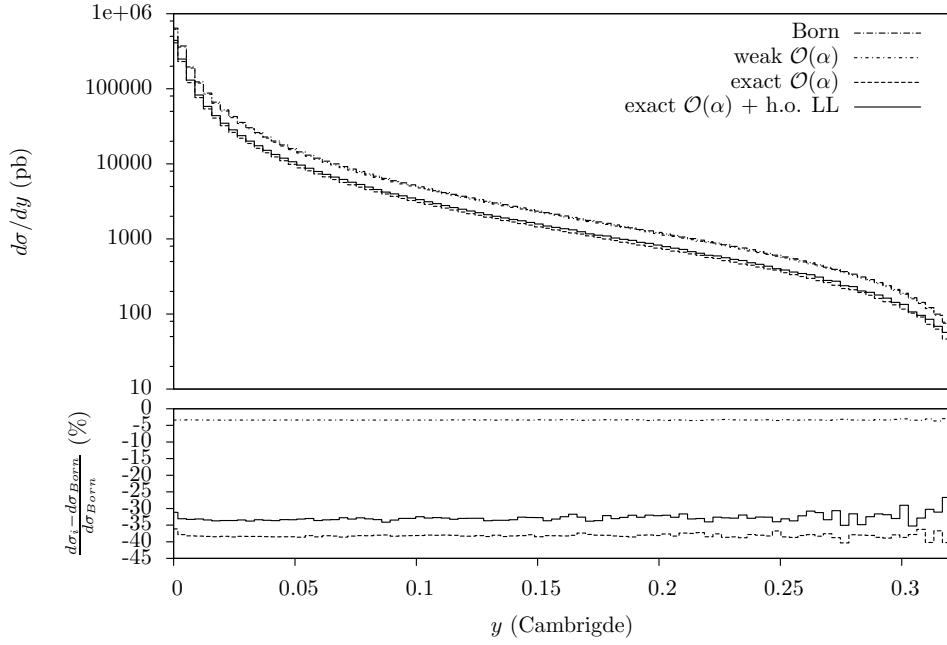
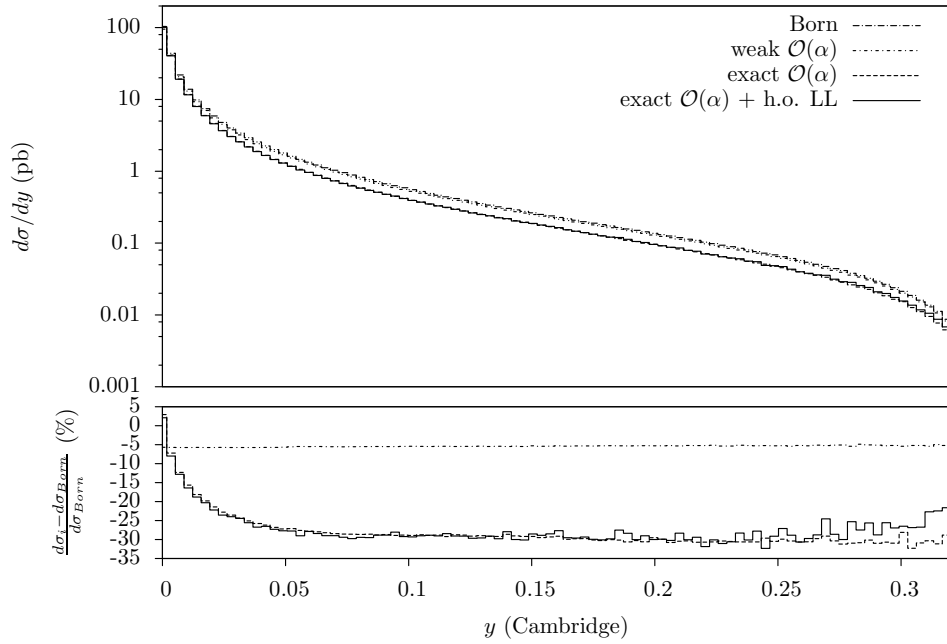**Figure 26**. Cambridge y distribution at the Z peak.

Figure 27. Cambridge y distribution at 350 GeV.

percent, depending on the energy and the observable being studied, and we have shown cases where such higher-order contributions would impinge on the experimental measurements of jet quantities.

A careful analysis of actual three-jet data is in order then, which should not only involve two-loop QCD contributions but also one-loop EW ones. One *caveat* should be
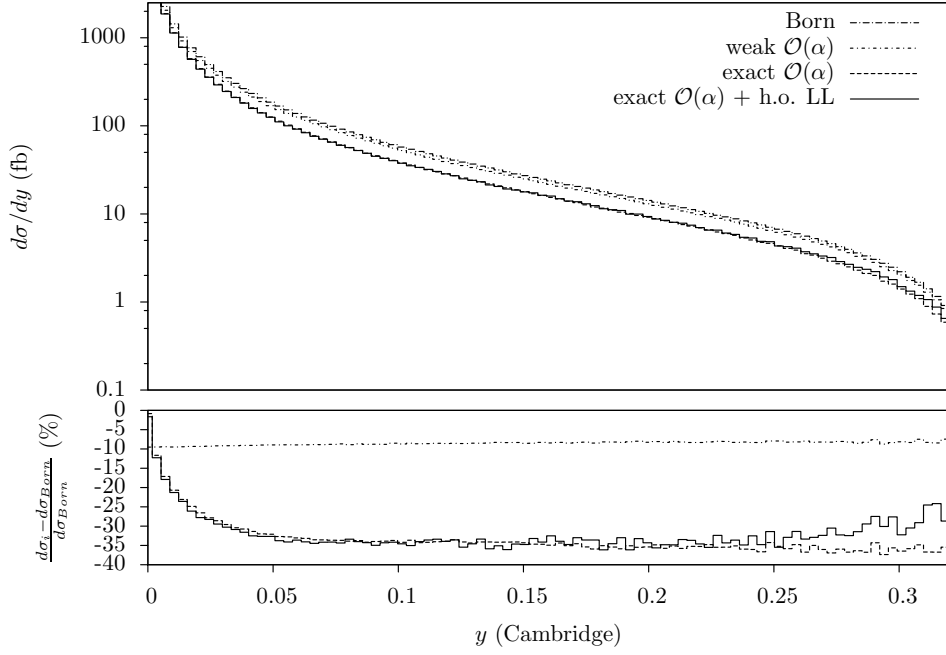
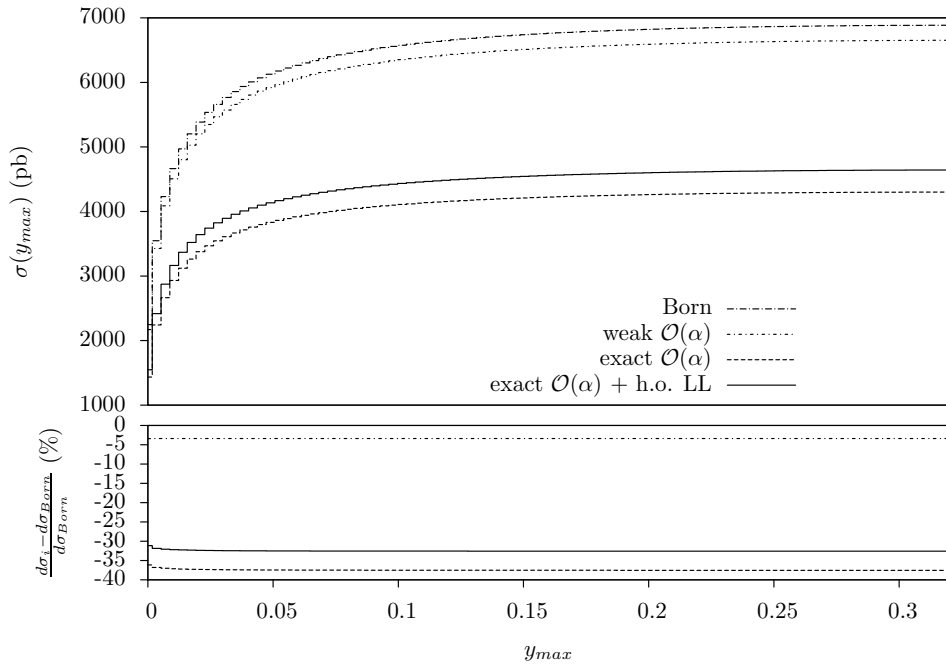**Figure 28**. Cambridge y distribution at $1\,\mathrm{TeV}$.

Figure 29. Integrated cross section as a function of the maximum y and relative corrections at the Z peak in the Cambridge scheme.

borne in mind though concerning the latter. That is, as emphasised in ref. [42], particular care should be devoted to the treatment of real $W^{\pm}$ and Z production and decay in the definition of the jet data sample, as this will determine whether tree-level $W^{\pm}$ and Z
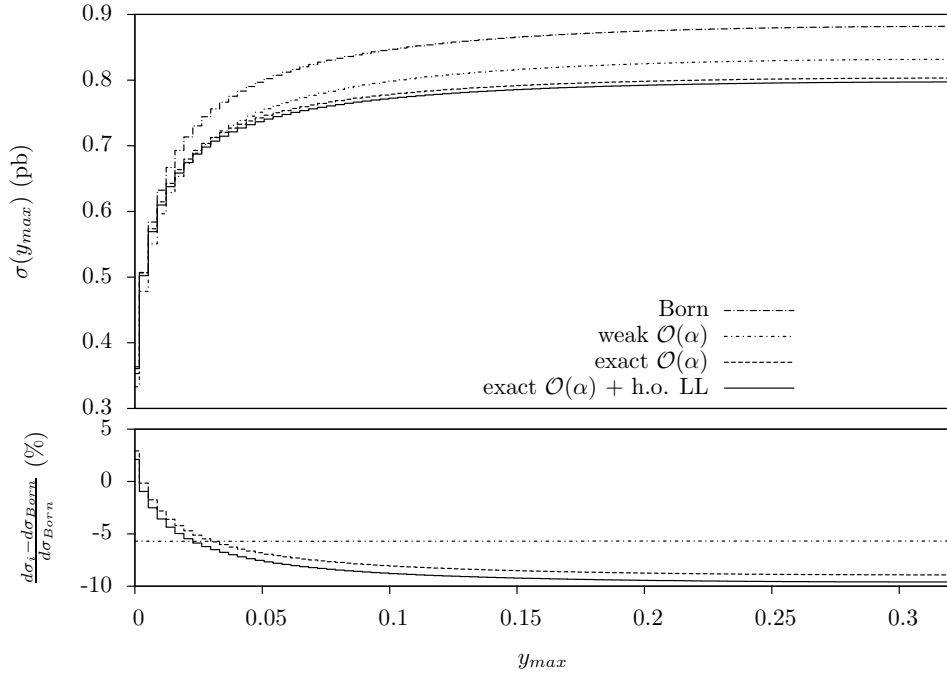
Figure 30. Integrated cross section as a function of the maximum y and relative corrections at 350 GeV in the Cambridge scheme.
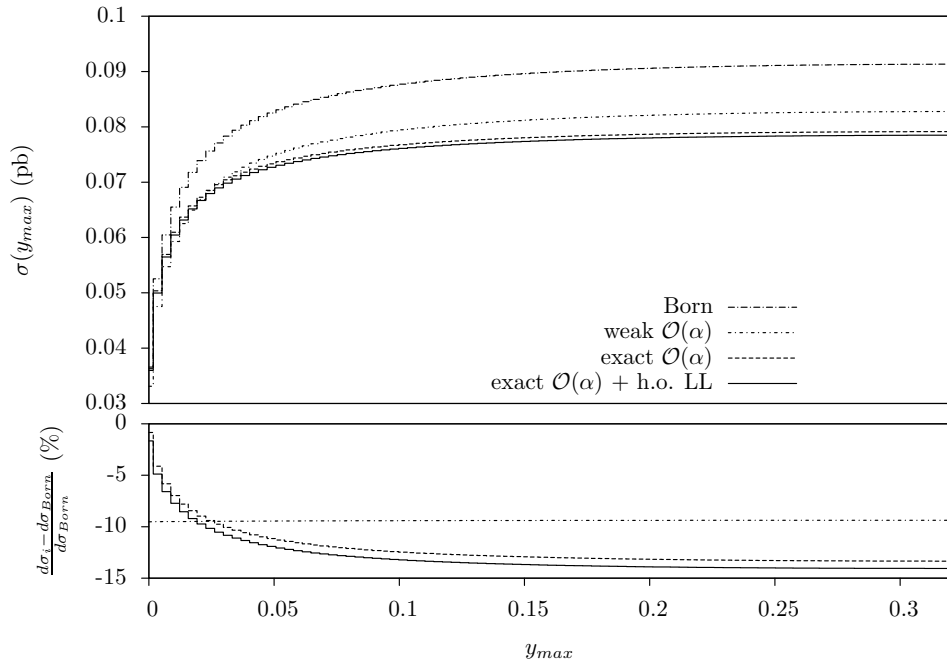

Figure 31. Integrated cross section as a function of the maximum y and relative corrections at 1 TeV in the Cambridge scheme.

bremsstrahlung effects (neglected here) have to be included in the theoretical predictions through $\mathcal{O}(\alpha_S \alpha_{EM}^3)$, which might counterbalance in part the effects due to one-loop $W^\pm$

and Z virtual exchange. However, given the cleanliness of leptonic jet data samples, as compared to hadronic ones, we believe that the former contribution can always be effectively disentangled in data.

We are now in the process of computing the $\mathcal{O}(\alpha_{\mathrm{S}}\alpha_{\mathrm{EM}}^3)$ one-loop QCD corrections to $e^+e^- \to q\bar{q}\gamma$, so that — upon combining these with the computations performed in this paper — we will eventually be in a position of rendering our complete predictions through that order of immediate experimental relevance.

Acknowledgments

A   Some useful formulas

In this appendix we display the analytic expressions for the IR divergent part of the relevant scalar integrals used in this work. Such divergences occur either in the case in which all the particles inside the loop are taken to be massless (zero-internal-mass integrals), such as box or pentagon graphs in which both the exchanged gauge bosons are photons, or graphs which contain one massive internal particle (one-internal-mass integrals) but are nevertheless IR divergent, such as box or pentagon graphs with one photon and one Z boson exchange. We perform the integrals in $(4-2\epsilon)$ dimensions with subtraction scale μ.

The zero-internal-mass integrals have been discussed in detail in, e.g., ref. [43], but for completeness we reproduce the results here, introducing some compact notation for integrals that will be used to describe the one-internal-mass integrals:

$$
\begin{aligned}
I_3^{(1,0)}(s) \equiv C_0(s,0,0,0,0,0) &\equiv \frac{1}{\pi^2} \int \frac{d^{(4-2\epsilon)}k}{k^2(k+p_1)^2(k+p_1+p_2)^2}\bigg|_{p_1^2=p_2^2=0,\ (p_1+p_2)^2=s} \\
&= \frac{r(\epsilon,\mu)}{\epsilon^2 s}\left(\frac{-s}{\mu^2}\right)^{-\epsilon},
\end{aligned}
\tag{A.1}
$$

where

$$
r(\epsilon,\mu) = \frac{\Gamma^2(1-\epsilon)\Gamma(1+\epsilon)}{\Gamma(1-2\epsilon)}\left(\pi\mu^2\right)^{-\epsilon} = \Gamma(1+\epsilon)\left(\pi\mu^2\right)^{-\epsilon}\left(1-\epsilon^2\frac{\pi^2}{6}+\cdots\right). \tag{A.2}
$$

$$
\begin{aligned}
I_3^{(2,0)}(s,t) \equiv C_0(s,t,0,0,0,0) &\equiv \frac{1}{\pi^2}\int\frac{d^{(4-2\epsilon)}k}{k^2(k+p_1)^2(k+p_1+p_2)^2}\bigg|_{p_1^2=t,\ p_2^2=0,\ (p_1+p_2)^2=s}\\
&= \frac{r(\epsilon,\mu)}{\epsilon^2(s-t)}\left(\left(\frac{-s}{\mu^2}\right)^{-\epsilon}-\left(\frac{-t}{\mu^2}\right)^{-\epsilon}\right),
\end{aligned}
\tag{A.3}
$$

$$I_4^{(1,0)}(s,t,p^2) \equiv D_0(s,t,p^2,0,0,0,0,0,0,0) \equiv \frac{1}{\pi^2} \int \frac{d^{(4-2\epsilon)}k}{k^2(k+p_1)^2(k+p_1+p_2)^2(k-p_4)^2}$$

$$= \frac{r(\epsilon,\mu)}{st} \left\{ \frac{2}{\epsilon^2} \left(\left(\frac{-s}{\mu^2}\right)^{-\epsilon} + \left(\frac{-t}{\mu^2}\right)^{-\epsilon} - \left(\frac{-p^2}{\mu^2}\right)^{-\epsilon} \right) \right.$$

$$\left. -2\mathrm{Li}_2\left(1-\frac{p^2}{s}\right) - 2\mathrm{Li}_2\left(1-\frac{p^2}{t}\right) - \ln\left(\frac{t}{s}\right)^2 - \frac{\pi^2}{3} \right\}. \qquad (A.4)$$

For the above box integral, $p_1^2 = p^2$, $p_i^2 = 0\,(i>1)$, $(p_1+p_2)^2 = s$, $(p_2+p_3)^2 = t$.

$$I_5^{(0,0)}(s_{12},s_{23},s_{34},s_{45},s_{51}) \equiv E_0(s_{12},s_{23},s_{34},s_{45},s_{51},0,0,0,0,0,0,0,0,0,0)$$

$$\equiv \frac{1}{\pi^2} \int \left. \frac{d^{(4-2\epsilon)}k}{k^2(k+p_1)^2(k+p_1+p_2)^2(k-p_4-p_5)^2(k-p_5)^2} \right|_{p_i^2=0,\ s_{ij}=2p_i\cdot p_j}$$

$$= \frac{-1}{s_{23}s_{34}s_{45}} \left\{ \frac{r(\epsilon,\mu)}{\epsilon^2} \left(\frac{-s_{23}s_{34}s_{45}}{s_{51}s_{12}\mu^2}\right)^{-\epsilon} + 2\mathrm{Li}_2\left(1-\frac{s_{23}}{s_{51}}\right) + 2\mathrm{Li}_2\left(1-\frac{s_{45}}{s_{12}}\right) - \frac{\pi^2}{6} \right\}$$

$$+ \text{cyclic permutations.} \qquad (A.5)$$

For the one-internal-mass-integrals, we begin with the IR divergent triangle integrals, i.e., those in which the internal massive propagator is adjacent to (as opposed to opposite) an external "mass".

$$I_3^{(1,1)}(s,M^2) \equiv C_0(s,0,0,M^2,0,0)$$

$$\equiv \frac{1}{\pi^2} \int \left. \frac{d^{(4-2\epsilon)}k}{(k^2-M^2)(k+p_1)^2(k+p_1+p_2)^2} \right|_{p_1^2=p_2^2=0,\ (p_1+p_2)^2=s}$$

$$= \frac{r(\epsilon,\mu)}{\epsilon^2 s} \left(\left(\frac{(M^2-s)}{\mu^2}\right)^{-\epsilon} - \left(\frac{M^2}{\mu^2}\right)^{-\epsilon} \right) - \frac{1}{s}\mathrm{Li}_2\left(\frac{s}{(s-M^2)}\right). \qquad (A.6)$$

$$I_3^{(2,1)}(s,t,M^2) \equiv C_0(s,t,0,0,0,0)$$

$$\equiv \frac{1}{\pi^2} \int \left. \frac{d^{(4-2\epsilon)}k}{(k^2-M^2)(k+p_1)^2(k+p_1+p_2)^2} \right|_{p_1^2=t,\ p_2^2=0,\ (p_1+p_2)^2=s}$$

$$= \frac{r(\epsilon,\mu)}{(s-t)} \left\{ \frac{1}{\epsilon^2} \left(\left(\frac{M^2-s}{\mu^2}\right)^{-\epsilon} - \left(\frac{M^2-t}{\mu^2}\right)^{-\epsilon} \right) - \mathrm{Li}_2\left(\frac{s}{(s-M^2)}\right) + \mathrm{Li}_2\left(\frac{t}{(t-M^2)}\right) \right\}.$$

$$\qquad (A.7)$$

We now show how the IR divergent part of an n-point integral can be obtained in terms of $(n-1)$-point integrals. This method is similar to that of ref. [44], but the resulting expressions are somewhat simpler. Consider an n-point integral with general incoming external momenta $p_i\ (i=1\cdots n)$ and a massive propagator on the line j_0,

$$I_n(p_1\cdots p_n,\ldots m_{j_0}\cdots) \equiv \frac{1}{\pi^2} \int \frac{d^{(4-2\epsilon)}k}{\prod_{j=0}^n \{(k+q_j)^2 - m_j^2\}}, \qquad (A.8)$$

where

$$q_j = \sum_{i=1}^j p_i, \quad q_0 = 0, \qquad (A.9)$$

and at least m_{j_0} is non-zero (there may, in general, be other internal finite masses, m_j).

After Feynman parameterisation the integral over the loop-momentum k may be performed yielding

$$I_n(p_1 \cdots p_n, \ldots m_{j_0} \cdots) = \Gamma(n + \epsilon - 2) \int \frac{\prod_j d\alpha_j \, \delta(1 - \sum_j \alpha_j)}{\left[\sum_{i,j}(q_i - q_j)^2 \alpha_i \alpha_j - m_{j_0}^2 \alpha_{j_0} - \cdots\right]^{n-2+\epsilon}}.$$ (A.10)

The integration over the Feynman parameters can only give rise to an IR divergence when $\alpha_{j_0} = 0$. In other words, the integral

$$\int \frac{\prod_j d\alpha_j \, \delta(1 - \sum_j \alpha_j) \alpha_{j_0}}{\left[\sum_{i,j}(q_i - q_j)^2 \alpha_i \alpha_j - m_{j_0}^2 \alpha_{j_0} - \cdots\right]^{n-2+\epsilon}}$$ (A.11)

is finite.

The term α_{j_0} in the numerator can be generated by considering the integral

$$\frac{1}{\pi^2} \int \frac{d^{(4-2\epsilon)} k \, 2 G_{j_0 l}^{-1} q_l \cdot k}{\prod_{j=0}^n \{(k + q_j)^2 - m_j^2\}},$$ (A.12)

where the Gram matrix, G, is defined by

$$G_{ij} = 2 q_i \cdot q_j.$$ (A.13)

Now, by using the "pinch" relations

$$2 q_l \cdot k = \left((k + q_l)^2 - m_l^2\right) - (k^2 - m_0^2) + m_l^2 - m_0^2 - q_l^2$$ (A.14)

and the fact that the integral (A.12) is IR finite, we obtain the result for the IR divergence part of the integral I_n,

$$\left\{\sum_l G_{j_0 l}^{-1} \left(m_l^2 - m_o^2 - q_l^2\right)\right\} I_n(p_1 \cdots p_n, \ldots m_{j_0} \cdots)|_{\text{IR}} = \sum_l G_{j_0 l}^{-1} \left(I_{(n-1)}^{\{l\}} - I_{(n-1)}^{\{0\}}\right),$$ (A.15)

where $I_{(n-1)}^{\{l\}}$ is the $(n-1)$-point integral obtained by "pinching out" the l-th propagator from the n-point integral, I_n.

Some of the integrals on the r.h.s. of eq. (A.15) may be IR convergent and may therefore be dropped. This process may then be iterated so that eventually the finite part of any integral with one internal mass can be expressed in terms of integrals with zero internal masses and the IR divergent triangle integrals.

The IR convergent contributions can then be obtained numerically, by taking the difference between the original IR divergent integrals on the r.h.s. of eq. (A.15) and regularising the divergences by inserting a small mass for all the internal propagators and then checking that the result is insensitive to the value taken for this regulator mass, provided it is much smaller than any of the other masses or momenta but not so small that it introduces numerical instabilities.

For the integrals required in this calculation, we have two IR box integrals with one non-zero internal mass and one non-zero external mass, depending on whether the external mass is opposite (a) or adjacent (b) to the massive propagator.

$$I_4^{(a)}(s,t,p^2,M^2) \equiv D_0(s,t,p^2,0,0,0,0,0,M^2,0)$$
$$\equiv \frac{1}{\pi^2} \int \frac{d^{(4-2\epsilon)}k}{k^2(k+p_1)^2((k+p_1+p_2)^2-M^2)(k-p_4)^2}, \quad \text{(A.16)}$$

with $p_1^2 = p^2$, $p_i^2 = 0\,(i>1)$, $(p_1+p_2)^2 = s$, $(p_2+p_3)^2 = t$.

$$I_4^{(b)}(s,t,p^2,M^2) \equiv D_0(s,t,0,p^2,0,0,0,0,M^2,0)$$
$$\equiv \frac{1}{\pi^2} \int \frac{d^{(4-2\epsilon)}k}{k^2(k+p_1)^2((k+p_1+p_2)^2-M^2)(k-p_4)^2}, \quad \text{(A.17)}$$

with $p_1^2 = 0$, $p_2^2 = p^2$ $p_i^2 = 0\,(i>2)$, $(p_1+p_2)^2 = s$, $(p_2+p_3)^2 = t$.

Using the above technique the IR divergent parts of these integrals are given by

$$I_4^{(a)}(s,t,p^2,M^2)_{\text{IR}} = \frac{sI_3^{(1,1)}(s,M^2) + (t-p^2)I_3^{(2,0)}(t,p^2)}{st - M^2(t-p^2)} \quad \text{(A.18)}$$

and

$$I_4^{(b)}(s,t,p^2,M^2)_{\text{IR}} = \frac{sI_3^{(1,1)}(s,M^2) + tI_3^{(1,0)}(t) + (s-p^2)I_3^{(2,1)}(s,p^2,M^2)}{t(s-M^2)}. \quad \text{(A.19)}$$

Finally we have the pentagon integral with no external masses and one internal mass, chosen arbitrarily to be the line between incoming momenta p_2 and p_3,

$$I_5^{(0,1)}(s_{12},s_{23},s_{34},s_{45},s_{51},M^2) \equiv E_0(s_{12},s_{23},s_{34},s_{45},s_{51},0,0,0,0,0,0,0,M^2,0,0)$$
$$\equiv \frac{1}{\pi^2} \int \frac{d^{(4-2\epsilon)}k}{k^2(k+p_1)^2((k+p_1+p_2)^2-M^2)k-p_4-p_5)^2(k-p_5)^2}\bigg|_{p_i^2=0,\ s_{ij}=2p_i\cdot p_j} \quad \text{(A.20)}$$

The IR divergent part of this integral is found to be

$$I_5^{0,1}(s_{12},s_{23},s_{34},s_{45},s_{51},M^2)_{\text{IR}} = \frac{1}{s_{51}s_{45}(s_{14}s_{25}+s_{12}s_{45}+2s_{12}s_{14}-s_{51}s_{24}-2M^2s_{14})}$$
$$\times \Big\{\big(s_{51}^2 s_{24} - s_{14}s_{51}s_{25} + s_{14}s_{51}s_{24} - s_{14}^2 s_{25} - s_{12}s_{51}s_{45} + s_{12}s_{14}s_{45}\big)I_4^{(a)}(s_{12},s_{23},s_{45},M^2)$$
$$+ \big(s_{12}s_{51}s_{45} - s_{51}^2 s_{24} + s_{14}s_{51}s_{25}\big)I_4^{(b)}(s_{12},s_{51},s_{34},M^2) + 2s_{14}s_{51}s_{45}I_4^{(1,0)}(s_{51},s_{45},s_{23})$$
$$+ \big(s_{51}s_{24}s_{45} + s_{14}s_{25}s_{45} - s_{14}s_{51}s_{24} + s_{14}^2 s_{25} - s_{12}s_{45}^2 - s_{12}s_{14}s_{45}\big)I_4^{(a)}(s_{34},s_{23},s_{51},M^2)$$
$$+ \big(s_{12}s_{45}^2 - s_{51}s_{24}s_{45} - s_{14}s_{25}s_{45} - 2s_{14}s_{51}s_{45}\big)I_4^{(b)}(s_{34},s_{45},s_{12},M^2)\Big\}. \quad \text{(A.21)}$$

References

[1] M. Kuroda, G. Moultaka and D. Schildknecht, *Direct one loop renormalisation of* $SU(2)_L \times U(1)_Y$ *four fermion processes and running coupling constants*, *Nucl. Phys.* **350** (1991) 25 [SPIRES];

G. Degrassi and A. Sirlin, *Gauge invariant selfenergies and vertex parts of the Standard Model in the pinch technique framework*, *Phys. Rev.* **46** (1992) 3104 [SPIRES];
A. Denner, S. Dittmaier and R. Schuster, *Radiative corrections to* $\gamma\gamma \to W^+W^-$ *in the electroweak standard model*, *Nucl. Phys.* **452** (1995) 80 [hep-ph/9503442] [SPIRES];
A. Denner, S. Dittmaier and T. Hahn, *Radiative corrections to* $ZZ \to ZZ$ *in the electroweak standard model*, *Phys. Rev.* **56** (1997) 117 [hep-ph/9612390] [SPIRES];
A. Denner and T. Hahn, *Radiative corrections to* $W^+W^- \to W^+W^-$ *in the electroweak standard model*, *Nucl. Phys.* **525** (1998) 27 [hep-ph/9711302] [SPIRES].

[2] W. Beenakker, A. Denner, S. Dittmaier, R. Mertig and T. Sack, *High-energy approximation for on-shell W pair production*, *Nucl. Phys.* **410** (1993) 245 [SPIRES];
W. Beenakker, A. Denner, S. Dittmaier and R. Mertig, *On shell W pair production in the TeV range*, *Phys. Lett.* **317** (1993) 622 [SPIRES].

[3] P. Ciafaloni and D. Comelli, *Sudakov enhancement of electroweak corrections*, *Phys. Lett.* **446** (1999) 278 [hep-ph/9809321] [SPIRES].

[4] A. Denner and S. Pozzorini, *One-loop leading logarithms in electroweak radiative corrections. I: results*, *Eur. Phys. J.* **C 18** (2001) 461 [hep-ph/0010201] [SPIRES].

[5] T. Kinoshita, *Mass singularities of Feynman amplitudes*, *J. Math. Phys.* **3** (1962) 650 [SPIRES];
T.D. Lee and M. Nauenberg, *Degenerate systems and mass singularities*, *Phys. Rev.* **133** (1964) B1549 [SPIRES].

[6] F. Bloch and A. Nordsieck, *Note on the radiation field of the electron*, *Phys. Rev.* **52** (1937) 54 [SPIRES].

[7] M. Ciafaloni, P. Ciafaloni and D. Comelli, *Bloch-Nordsieck violating electroweak corrections to inclusive TeV scale hard processes*, *Phys. Rev. Lett.* **84** (2000) 4810 [hep-ph/0001142] [SPIRES].

[8] See e.g. M. Consoli, W. Hollik and F. Jegerlehner, *Electroweak radiative corrections for Z physics*, in *Proceedings of the workshop "Z Physics at LEP1"*, G. Altarelli, R. Kleiss and C. Verzegnassi eds., preprint CERN-89-08 [CERN-TH-5527-89] [SPIRES] (1989) and references therein.

[9] V.A. Khoze, D.J. Miller, S. Moretti and W.J. Stirling, *Hadronic returns to the Z in electron-positron annihilation at high energy*, *JHEP* **07** (1999) 014 [hep-ph/9906334] [SPIRES].

[10] E. Maina, S. Moretti, M.R. Nolten and D.A. Ross, *Weak corrections to hadronic observables*, hep-ph/0407150 [SPIRES];
E. Maina, S. Moretti and D.A. Ross, *One-loop weak corrections to three-jet observables at the Z pole*, hep-ph/0403269 [SPIRES].

[11] U. Baur, *Weak boson emission in hadron collider processes*, *Phys. Rev.* **D 75** (2007) 013005 [hep-ph/0611241] [SPIRES].

[12] ILC collaboration, A. Djouadi et al., *International Linear Collider reference design report volume 2: physics at the ILC*, arXiv:0709.1893 [SPIRES];
ACFA LINEAR COLLIDER WORKING GROUP collaboration, K. Abe et al., *Particle physics experiments at JLC*, hep-ph/0109166 [SPIRES];
AMERICAN LINEAR COLLIDER WORKING GROUP collaboration, T. Abe et al., *Linear collider physics resource book for Snowmass* 2001. 1: *introduction*, hep-ex/0106055

[SPIRES]; *Linear collider physics resource book for Snowmass* 2001. 2*: Higgs and supersymmetry studies*, `hep-ex/0106056` [SPIRES]; *Linear collider physics resource book for Snowmass* 2001. 3*: studies of exotic and standard model physics*, `hep-ex/0106057` [SPIRES]; *Linear collider physics resource book for Snowmass* 2001. 4*: theoretical, accelerator and experimental options*, `hep-ex/0106058` [SPIRES];

ECFA/DESY LC PHYSICS WORKING GROUP collaboration, J.A. Aguilar-Saavedra et al., *TESLA technical design report part III: physics at an e^+e^- linear collider*, `hep-ph/0106315` [SPIRES];

CLIC STUDY TEAM collaboration, G. Guignard et al. eds., *A 3 TeV e^+e^- linear collider based on CLIC technology*, preprint CERN-2000-008 [SPIRES] (2000).

[13] G. Dissertori, *Measurements of α_s from event shapes and the four- jet rate*, `hep-ex/0209070` [SPIRES] and reference therein;
LEP ELECTROWEAK WORKING GROUP collaboration, *The LEP Electroweak Working Group homepage*, http://www.cern.ch/LEPEWWG.

[14] M. Winter, *Determination of the strong coupling constant at Giga-Z*, LC Note LC-PHSM-2001-016 [SPIRES] (2001) and references therein.

[15] A. Gehrmann-De Ridder, T. Gehrmann, E.W.N. Glover and G. Heinrich, *Jet rates in electron-positron annihilation at $O(\alpha_s^3)$ in QCD*, *Phys. Rev. Lett.* **100** (2008) 172001 [`arXiv:0802.0813`] [SPIRES]; *Event shapes in e^+e^- annihilation at NNLO*, `PoS(RADCOR2007)048` [`arXiv:0801.2680`] [SPIRES]; *NNLO corrections to event shapes in e^+e^- annihilation*, *JHEP* **12** (2007) 094 [`arXiv:0711.4711`] [SPIRES]; *Infrared structure of $e^+e^- \to 3$ jets at NNLO*, *JHEP* **11** (2007) 058 [`arXiv:0710.0346`] [SPIRES]; *NNLO QCD corrections to event shape variables in electron positron annihilation*, *J. Phys. Conf. Ser.* **110** (2008) 022014 [`arXiv:0709.4221`] [SPIRES]; *First results on $e^+e^- \to 3$ jets at NNLO*, *eConf* **C0705302** (2007) TOP10 [`arXiv:0709.1608`] [SPIRES]; *Second-order QCD corrections to the thrust distribution*, *Phys. Rev. Lett.* **99** (2007) 132002 [`arXiv:0707.1285`] [SPIRES]; *Infrared structure of $e^+e^- \to 3$ jets at NNLO: QED-type contributions*, *Nucl. Phys. Proc. Suppl.* **160** (2006) 190 [`hep-ph/0607042`] [SPIRES];
A. Gehrmann-De Ridder, T. Gehrmann and E.W.N. Glover, *Infrared structure of $e^+e^- \to 3$ jets at NNLO - the C_F^2 contribution*, *Nucl. Phys. Proc. Suppl.* **135** (2004) 97 [`hep-ph/0407023`] [SPIRES];
L.W. Garland, T. Gehrmann, E.W.N. Glover, A. Koukoutsakis and E. Remiddi, *Two-loop QCD helicity amplitudes for $e^+e^- \to 3$ jets*, *Nucl. Phys.* **B 642** (2002) 227 [`hep-ph/0206067`] [SPIRES]; *The two-loop QCD matrix element for $e^+e^- \to 3$ Jets*, *Nucl. Phys.* **B 627** (2002) 107 [`hep-ph/0112081`] [SPIRES].

[16] R.K. Ellis, D.A. Ross and A.E. Terrano, *The perturbative calculation of jet structure in e^+e^- annihilation*, *Nucl. Phys.* **178** (1981) 421 [SPIRES].

[17] S. Moretti, R. Muñoz-Tapia and J.B. Tausk, *Heavy flavour tagging and QCD tests in four-jet events at LEP*1, `hep-ph/9609206` [SPIRES];
S. Moretti and J.B. Tausk, *QCD effects and B tagging at LEP*1, *Z. Phys.* **C 69** (1996) 635 [`hep-ph/9503354`] [SPIRES].

[18] C.M. Carloni Calame, S. Moretti, F. Piccinini and D.A. Ross, *One-loop electroweak corrections to e^+e^- into three-jets*, `PoS(RADCOR2007)004` [`arXiv:0804.1657`] [SPIRES].

[19] G. Passarino and M.J.G. Veltman, *One loop corrections for e^+e^- annihilation into $\mu^+\mu^-$ in the Weinberg model*, *Nucl. Phys.* **B 160** (1979) 151 [SPIRES].

[20] J.A.M. Vermaseren, *New features of FORM*, `math-ph/0010025` [SPIRES].

[21] A. Denner, S. Dittmaier, M. Roth and D. Wackeroth, *Predictions for all processes* $e^+e^- \to$ *fermions* $+\gamma$, *Nucl. Phys.* **560** (1999) 33 [SPIRES];
A. Denner, S. Dittmaier, M. Roth and L.H. Wieders, *Electroweak corrections to charged-current* $e^+e^- \to 4$ *fermion processes: technical details and further results*, *Nucl. Phys.* **724** (2005) 247 [SPIRES];
A. Denner and S. Dittmaier, *The complex-mass scheme for perturbative calculations with unstable particles*, *Nucl. Phys. Proc. Suppl.* **160** (2006) 22 [`hep-ph/0605312`] [SPIRES].

[22] A.A. Pivovarov, *Running electromagnetic coupling constant: low energy normalization and the value at M(Z)*, *Phys. Atom. Nucl.* **65** (2002) 1319 [*Yad. Fiz.* **65** (2002) 1352] [`hep-ph/0011135`] [SPIRES].

[23] M. Green and M.J.G. Veltman, *Weak and electromagnetic radiative corrections to low-energy processes*, *Nucl. Phys.* **B 169** (1980) 137 [*Erratum ibid.* **B 175** (1980) 547] [SPIRES].

[24] T. Hahn and M. Pérez-Victoria, *Automatized one-loop calculations in four and D dimensions*, *Comput. Phys. Commun.* **118** (1999) 153 [`hep-ph/9807565`] [SPIRES].

[25] A. Denner and S. Dittmaier, *Reduction of one-loop tensor 5-point integrals*, *Nucl. Phys.* **B 658** (2003) 175 [`hep-ph/0212259`] [SPIRES].

[26] G.J. van Oldenborgh, *FF — a package to evaluate one-loop Feynman diagrams*, *Comp. Phys. Commun.* **66** (1991) 1 [SPIRES].

[27] F. Caravaglios and M. Moretti, *An algorithm to compute Born scattering amplitudes without Feynman graphs*, *Phys. Lett.* **B 358** (1995) 332 [`hep-ph/9507237`] [SPIRES].

[28] T. Stelzer and W.F. Long, *Automatic generation of tree level helicity amplitudes*, *Nucl. Phys. Proc. Suppl.* **37B** (1994) 158 [SPIRES].

[29] A. Ballestrero, E. Maina and S. Moretti, *Heavy quark production at* e^+e^- *colliders in three and four jet events*, *Phys. Lett.* **B 294** (1992) 425 [SPIRES]; *Heavy quarks and leptons at* e^+e^- *colliders*, *Nucl. Phys.* **B 415** (1994) 265 [`hep-ph/9212246`] [SPIRES].

[30] G. Balossini, C.M. Carloni Calame, G. Montagna, O. Nicrosini and F. Piccinini, *Matching perturbative and parton shower corrections to Bhabha process at flavour factories*, *Nucl. Phys.* **B 758** (2006) 227 [`hep-ph/0607181`] [SPIRES].

[31] E.A. Kuraev and V.S. Fadin, *On radiative corrections to* e^+e^- *single photon annihilation at high-energy*, *Sov. J. Nucl. Phys.* **41** (1985) 466 [*Yad. Fiz.* **41** (1985) 733] [SPIRES];
G. Altarelli and G. Martinelli, *Radiative corrections to the Z0 line shape at LEP*, in *Physics at LEP*, vol. 1, J. Ellis and R. Peccei eds., CERN Report 86-02, Geneva Switzerland (1986), pg. 47 [SPIRES];
O. Nicrosini and L. Trentadue, *Soft photons and second order radiative corrections to* $e^+e^- \to Z0$, *Phys. Lett.* **B 196** (1987) 551 [SPIRES]; *Second order electromagnetic radiative corrections to* $e^+e^- \to \gamma*$, $Z0 \to \mu^+\mu^-$, *Z. Phys.* **C 39** (1988) 479 [SPIRES].

[32] G. Montagna, O. Nicrosini and F. Piccinini, $O(\alpha^2)$ *next-to-leading photonic corrections to small angle Bhabha scattering in the structure function formalism*, *Phys. Lett.* **B 385** (1996) 348 [`hep-ph/9605252`] [SPIRES].

[33] G. 't Hooft and M.J.G. Veltman, *Scalar one-loop integrals*, *Nucl. Phys.* **B 153** (1979) 365 [SPIRES].

[34] See for instance W. Beenakker et al., *The fermion loop scheme for finite width effects in* e^+e^- *annihilation into four fermions*, *Nucl. Phys.* **B 500** (1997) 255 [`hep-ph/9612260`] [SPIRES].

[35] Y.L. Dokshitzer, G.D. Leder, S. Moretti and B.R. Webber, *Better jet clustering algorithms*, *JHEP* **08** (1997) 001 [hep-ph/9707323] [SPIRES];
S. Moretti, L. Lönnblad and T. Sjöstrand, *New and old jet clustering algorithms for electron-positron events*, *JHEP* **08** (1998) 001 [hep-ph/9804296] [SPIRES].

[36] S. Brandt, C. Peyrou, R. Sosnowski and A. Wroblewski, *The principal axis of jets — an attempt to analyse high-energy collisions as two-body processes* , *Phys. Lett.* **12** (1964) 57 [SPIRES];
E. Farhi, *A QCD test for jets*, *Phys. Rev. Lett.* **39** (1977) 1587 [SPIRES].

[37] H. Georgi and M. Machacek, *A simple QCD prediction of jet structure in e^+e^- annihilation*, *Phys. Rev. Lett.* **39** (1977) 1237 [SPIRES].

[38] R.K. Ellis, D.A. Ross and A.E. Terrano, *The perturbative calculation of jet structure in e^+e^- annihilation*, *Nucl. Phys.* **B 178** (1981) 421 [SPIRES].

[39] MARK-J collaboration, D.P. Barber et al., *Discovery of three jet events and a test of quantum chromodynamics at PETRA energies*, *Phys. Rev. Lett.* **43** (1979) 830 [SPIRES].

[40] ALEPH collaboration, G. Dissertori, *QCD studies with e^+e^- annihilation data at 189 GeV*, prepared for the *International Europhysics Conference on High-Energy Physics (EPS-HEP 99)*, Tampere Finland July 15–21 1999, ALEPH-99-023 [CONF-99-018] [SPIRES] (1999).

[41] See e.g. Z. Kunszt and P. Nason, *QCD at LEP*, in *Proceedings of the workshop "Z Physics at LEP1"*, G. Altarelli, R. Kleiss and C. Verzegnassi eds., preprint CERN-89-08 (1989) [SPIRES] and references therein.

[42] S. Moretti, M.R. Nolten and D.A. Ross, *Weak corrections and high E_T jets at Tevatron*, *Phys. Rev.* **D 74** (2006) 097301 [hep-ph/0503152] [SPIRES]; *Weak effects in proton beam asymmetries at polarised RHIC and beyond*, *Phys. Lett.* **B 643** (2006) 86 [hep-ph/0509254] [SPIRES]; *Weak corrections to gluon-induced top-antitop hadro-production*, *Phys. Lett.* **B 639** (2006) 513 [hep-ph/0603083] [SPIRES]; *Weak corrections to four-parton processes*, *Nucl. Phys.* **B 759** (2006) 50 [hep-ph/0606201] [SPIRES];
E. Maina, S. Moretti, M.R. Nolten and D.A. Ross, *One-loop weak corrections to the $b\bar{b}$ cross section at TeV energy hadron colliders*, *Phys. Lett.* **B 570** (2003) 205 [hep-ph/0307021] [SPIRES].

[43] Z. Bern, L.J. Dixon and D.A. Kosower, *Dimensionally regulated pentagon integrals*, *Nucl. Phys.* **B 412** (1994) 751 [hep-ph/9306240] [SPIRES].

[44] S. Dittmaier, *Separation of soft and collinear singularities from one-loop N-point integrals*, *Nucl. Phys.* **B 675** (2003) 447 [hep-ph/0308246] [SPIRES].

[45] E. Maina, S. Moretti and D.A. Ross, *Weak corrections to three-jet production in electron positron annihilations*, *JHEP* **04** (2003) 056 [hep-ph/0210015] [SPIRES].

Erratum

All the integrated and differential cross-sections presented in the original paper have been mistakenly multiplied by an overall factor of 1/3. Furthermore, besides the cuts described in section 4, an additional cut was imposed to obtain the results which is not correctly stated in the paper: namely, the energy of each jet is required to be larger than $\min(5\text{GeV}, 0.05 \times \sqrt{s})$.

However, the relative effects due to the impact of the full one-loop EW terms of $\mathcal{O}(\alpha_{\text{S}}\alpha_{\text{EM}}^3)$ remain unchanged as well as the conclusions of our study.

Added acknowledgments

We gratefully acknowledge an email exchange with Ansgar Denner, Stefan Dittmaier, Thomas Gehrmann and Christian Kurz [46] and thank them for pointing out the discrepancy with their independent calculation.

Added references

[46] A. Denner, S. Dittmaier, T. Gehrmann and C. Kurz, *Electroweak corrections to three-jet production in electron-positron annihilation*, `arXiv:0906.0372`; private communication.

JHEP03(2009)047